

CHAPTER 6

SCINTILLATION COUNTING

6.1 Scintillator-photomultiplier combination

- 6.1.1 Scintillator shape
- 6.1.2 Scintillator finish
- 6.1.3 Scintillator-photomultiplier coupling

6.2 Electrical signal characteristics

- 6.2.1 Current pulse
- 6.2.2 Voltage pulse

6.3 Operating mode

- 6.3.1 Continuous mode
- 6.3.2 Pulse mode

Appendix Scintillator fundamentals

- A6.1 Inorganic scintillators
- A6.2 Organic scintillators
- A6.3 Scintillator characteristics
- A6.4 Scintillator properties
 - A6.4.1 Inorganic-scintillator properties
 - A6.4.2 Organic-scintillator properties

SCINTILLATION COUNTING

Nuclear radiation absorbed in certain materials excites flashes of light – scintillations. The first laboratory application of this phenomenon was the spintharoscope, in which scintillations of a zinc sulphide screen are observed through a microscope. Early twentieth century investigators who patiently counted the scintillations excited by different radioactive substances, thereby helping to lay the foundations for today's understanding of radioactivity, were the first scintillation counters.

Depending critically as it did on a trained observer's eye and powers of concentration, the spintharoscope was an instrument of inherently limited usefulness. What put scintillation counting on a practical footing was the invention of the photomultiplier, the development of electronic circuits to exploit the photomultiplier's capabilities, and the formulation of more efficient scintillators. Together, these freed it from the constraints of the research laboratory and made it accessible to a varied range of scientific and industrial applications.

Today, scintillation counting is routine and widely used: not only in high-energy and radiation physics research but also in medicine, for diagnostic imaging and analysis, and in industry for thickness and density measurement, non-destructive analysis, and oil-well logging.

6.1 Scintillator-photomultiplier combination

Unlike the zinc sulphide screen, nearly all present-day scintillators are transparent. How much of the light from such a scintillator reaches the photomultiplier cathode depends on the shape, absorption, refractive index and surface finish of the scintillator, and how it is coupled to the cathode window. (Liquid scintillators, a special case, are considered in §7.2.1)

6.1.1 Scintillator shape

Scintillation photons are emitted in all directions; some reach the cathode directly, others by internal reflection. The best scintillator shape is one in which the total number of photons reaching the cathode is maximum and the number of internal reflections minimum; efficiencies of various scintillator shapes are dealt with extensively in the literature and in suppliers' catalogues. For many applications, truncated-cone and parabolic shapes give the most satisfactory results, but simple shapes like rods and blocks, which are less expensive to fabricate, are often good enough. Lately, scintillating fibres have become commercially available.

6.1.2 Scintillator finish

The surface finish and symmetry of the scintillator determine how much light escapes from it or is internally absorbed before reaching the photomultiplier cathode. Losses tend to be higher in highly symmetrical scintillators. They can be lessened by spoiling the symmetry or altering the finish of some surfaces, for instance by roughening or applying a reflective coating to them.

In long scintillators multiple internal reflections play an important role in transporting light from one end to the other. Scintillation plates are an example; the parallel surfaces should be polished to promote reflection and, in some cases, reflectively coated. The most suitable coatings are MgO, TiO₂, and Al. Figure 6.1 shows the reflection coefficients of these materials as a function of wavelength.

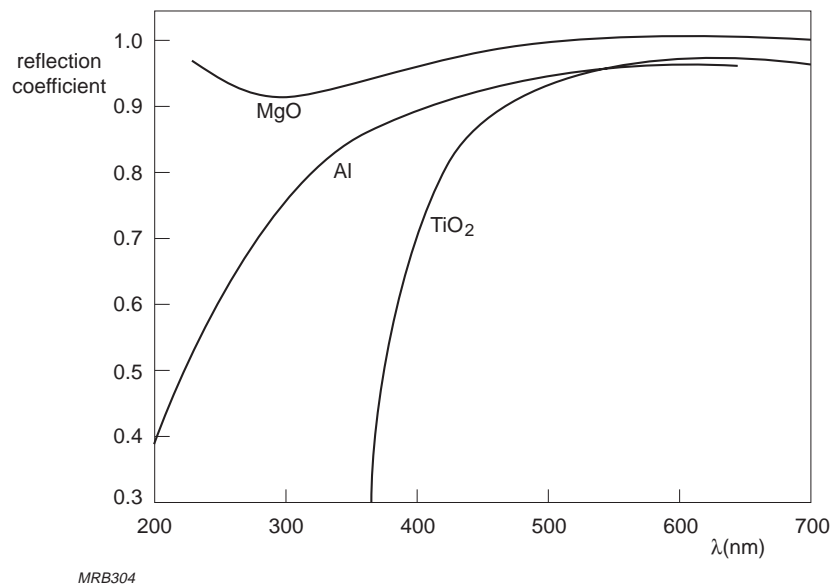
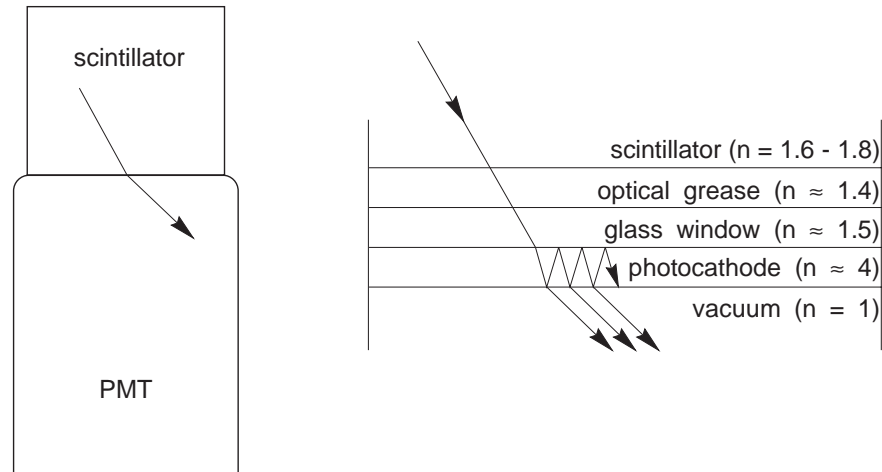


Fig.6.1 Reflection coefficients of aluminium, titanium dioxide and manganese oxide as functions of wavelength

6.1.3 Scintillator-photomultiplier coupling

The way the scintillator is coupled to the photomultiplier affects the proportion of photons that reach the cathode. Coupling efficiency is especially important in spectrometry, where maximum photon collection is essential. The fact that a semi-transparent cathode has a higher refractive index than the glass and vacuum on either side of it is fortunate; it encourages multiple internal reflections inside the cathode and so increases the probability of photoemission (Fig.6.2).



MRB305

Fig.6.2 Light transmission through the window and through the photocathode

Direct coupling. If the scintillator output surface is no larger than the cathode window, the two can simply be butted together. Use of a mating compound such as silicone grease, with a refractive index close to the refractive indices of the scintillator and the glass, is necessary to minimize interface losses.

Light-guide coupling. When it is not practical to couple the scintillator direct to the cathode window, either because its output surface is too large or too small or inconveniently shaped, or because operating circumstances necessitate keeping the two apart, a light guide has to be used. The usual materials are glass, fused silica, polystyrene, polyvinyltoluene, and especially polymethyl methacrylate (Perspex*, Lucite*, Plexiglass*, Altuglas*). The last named is less UV transparent than fused silica, but it has the advantage of being much easier to fabricate (Fig.6.3).

* Registered trademark

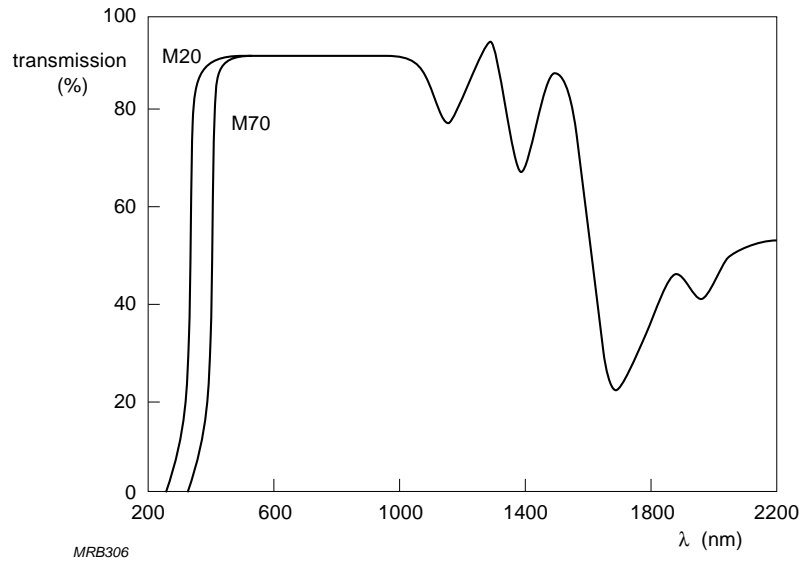
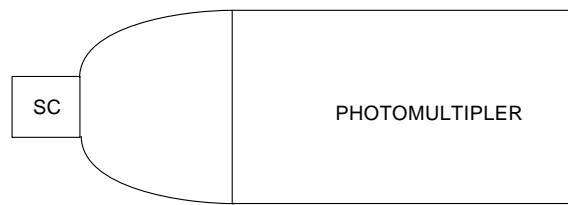
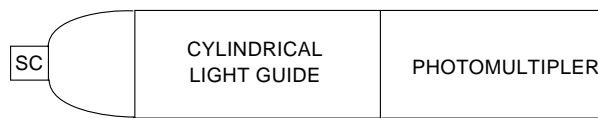


Fig.6.3 Transmission coefficient of Altuglas (composition M20 and M70) as a function of wavelength



(a)



(b)

MRB307

Fig.6.4 Logarithmic-spiral light guide (a) between scintillator and PMT, (b) with an intermediate cylindrical light guide

When the scintillator output surface is smaller than the cathode window, light guides with logarithmic-spiral (Fig.6.4), parabolic, or other special shapes can theoretically provide coupling efficiencies of 100%. In practice, however, losses due to internal reflection and absorption usually reduce that to something closer to 70%.

If the size and shape of the scintillator output surface are comparable to those of the cathode window, the light guide is cylindrical. Losses in such a light guide are characterized by an *attenuation length* in which the light intensity is halved; for a 25 mm diameter cylinder of polished methacrylate the attenuation length for visible light is more than a metre. Attenuation length is wavelength dependent and can be increased by using wavelength shifters (e.g. BBQ, K27, Y7 etc.) to shift the scintillation light to longer wavelengths, see below.

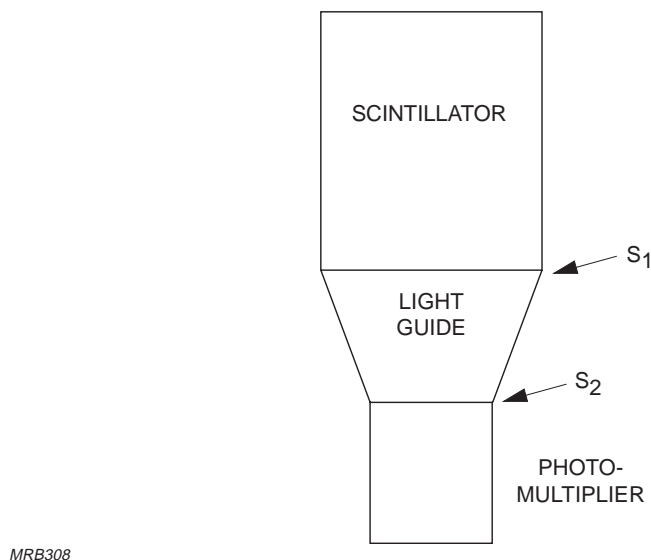
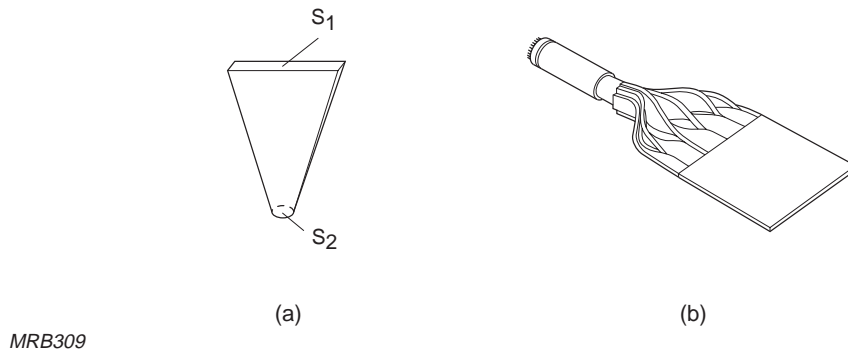


Fig.6.5 Truncated cone light guide

When the scintillator output surface is larger than the cathode window no light-guide shape is even theoretically 100% efficient. The best and most popular compromise is a truncated cone (Fig.6.5). Optimum design calls for a trade-off between the included angle of the cone and its length. The larger the angle, the sooner the internal reflections reach the critical angle of incidence and escape through the lateral surface of the light guide. On the other hand, the smaller the angle, the longer the light guide and the larger the absorption losses. The coupling efficiency never exceeds the ratio of the cathode area to the scintillator output area (S_2/S_1 , Fig.6.5). Therefore, the only practical application for such a light guide is when operating circumstances

necessitate having the scintillator remote from the cathode window; when that is not the case, direct coupling works just as well.

The fishtail and strip-light illustrated in Fig.6.6 are two examples of light guides designed to adapt specially shaped scintillators to circular cathode windows. Many others are described in the literature.



MRB309

Fig.6.6 The fishtail (a) and strip-light (b) are two examples of light guides designed to adapt specially shaped scintillators to circular cathode windows

Wavelength shifters. Particle physics experiments often use large scintillator plates that cannot be coupled direct to a photomultiplier; moreover, the light they emit is toward the blue end of the spectrum, where the transmission of most light guides is far from good. To overcome this difficulty, transparent media incorporating fluorescent substances are used that shift the colour toward the green, yellow, or red, where transmission is better. The well-known wavelength shifters BBQ, Y7 and K27 shift blue scintillation light into the green part of the spectrum where tubes with extended green sensitivity bialkali cathodes have good sensitivity. Tubes with S20 cathodes could also be used, but price considerations normally limit them to use only with yellow or red wavelength shifters. Use of different fluorescent substances in different parts of a wavelength shifter can make particle discrimination possible.

Wavelength shifters usually take the form of a bar or a sheet air-coupled to the scintillator. It may, in fact, integrate the light from many scintillators and may be coupled to a separate light guide or itself serve as one. Wavelength-shifting fibres are gaining in popularity despite their low efficiency when used, for example, together with flat scintillators.

Wavelength-shifting layers can also be deposited on the photomultiplier window. The main disadvantages of this are low efficiency, loss of time resolution and degraded linearity.

6.2 Electrical signal characteristics

6.2.1 Current pulse

The light emission $L(t)$ of a scintillator excited at time $t = 0$ can be approximated by

$$L(t) = \frac{\bar{n}_{p,s}}{\tau} \exp\left(-\frac{t}{\tau}\right)$$

where $\bar{n}_{p,s}$ is the mean number of photons per scintillation and τ is the decay time constant of the scintillator. The resulting number of electrons at the photomultiplier anode is given by the convolution product

$$S(t) = L(t) * R_{\delta}(t)$$

where $R_{\delta}(t)$ is the photomultiplier pulse response. If the photomultiplier response-pulse width t_w is negligible compared with τ , this reduces to

$$S(t) \approx \frac{\bar{n}_{a,s}}{\tau} \exp\left(-\frac{t}{\tau}\right)$$

where $\bar{n}_{a,s}$ is the mean number of anode electrons per scintillation; or, in terms of the anode current I_a and anode charge $q_{a,s}$

$$I_a(t) = \frac{\bar{q}_{a,s}}{\tau} \exp\left(-\frac{t}{\tau}\right) \quad (6.1)$$

6.2.2. Voltage pulse

In the circuit of Fig.6.7 the current pulse of Eq.6.1 gives rise to a voltage pulse

$$V_a(t) = \frac{\bar{q}_{a,s}}{C} \frac{\theta}{\tau - \theta} \left\{ \exp\left(-\frac{t}{\tau}\right) - \exp\left(-\frac{t}{\theta}\right) \right\} \quad (6.2)$$

where $\theta = R_L C$. Figure 6.8 shows the pulse shape; the amplitude is given by

$$V_a = \frac{\bar{q}_{a,s}}{C} \left(\frac{\theta}{\tau} \right)^{\frac{1}{1 - \frac{\theta}{\tau}}}$$

As θ/τ tends toward infinity, V_a tends toward the limit $\bar{q}_{a,s}/C$. Figure 6.9 shows the effect of θ/τ on relative amplitude, and Fig.6.10 its effect on pulse shape; in Fig.6.11 the curves of Fig.6.10 are normalized to unit amplitude. Figure 6.12 shows the

variation of rise time with θ/τ , and Fig.6.13 the variation of full width at half maximum, in both cases normalized with respect to τ .

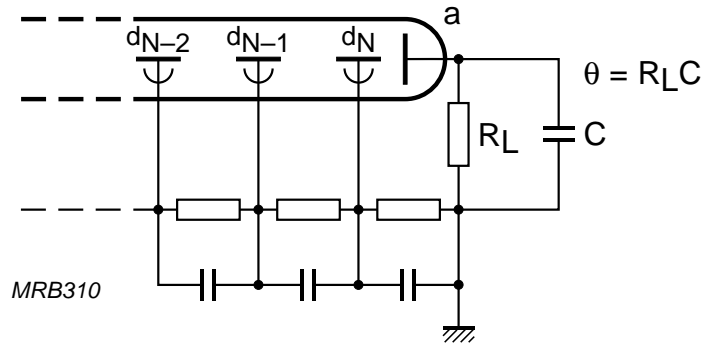


Fig.6.7 Anode circuit with the anode load $R_L C$

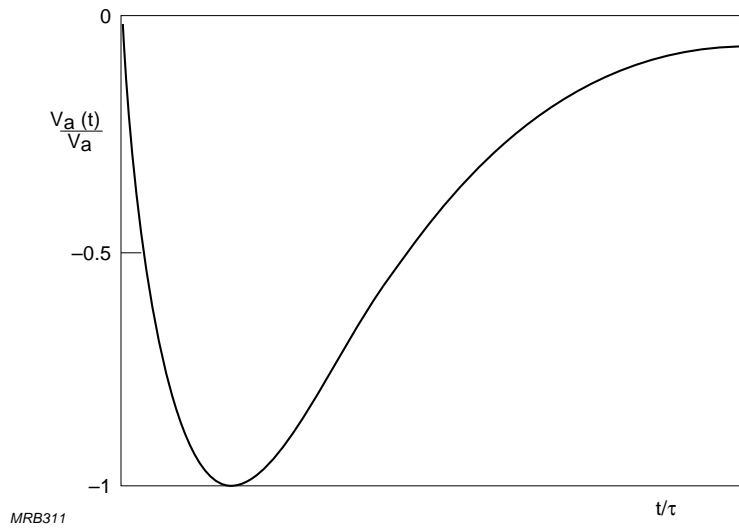


Fig.6.8 Voltage pulse shape over the anode load $R_L C$

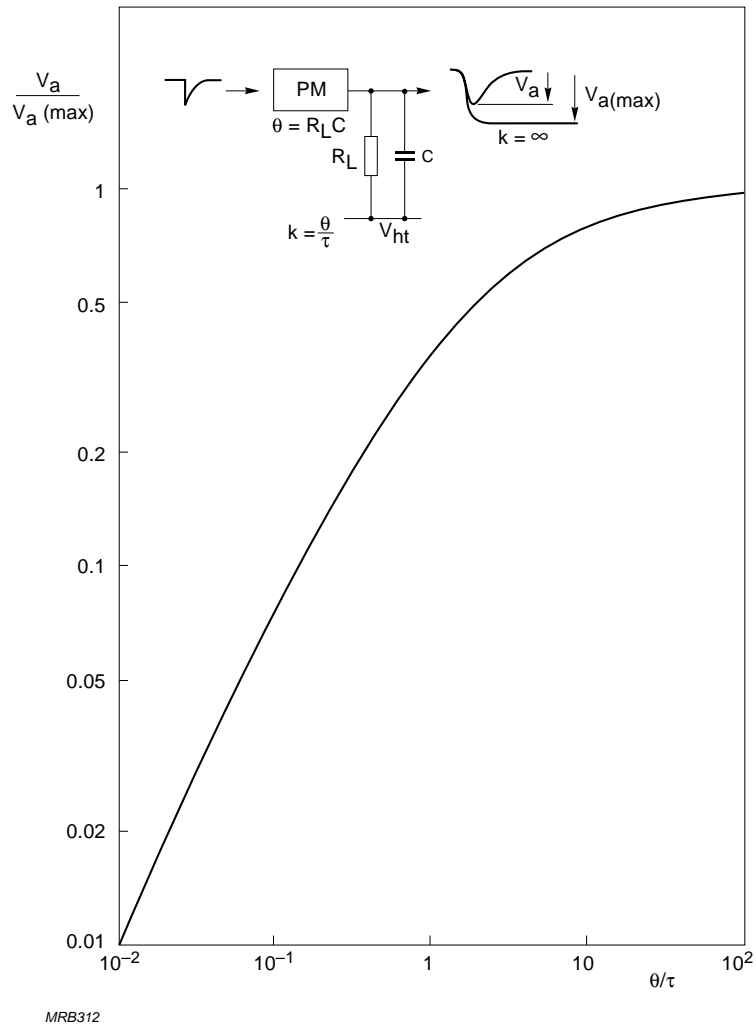


Fig. 6.9 Relative pulse amplitude variations as a function of the ratio θ/τ , τ being the scintillator decay time constant

Special cases

When $\theta \ll \tau$, Eq.6.2 approaches the limit

$$V_a(t) = \frac{\bar{q}_{a,s}}{C} \frac{\theta}{\tau} \left\{ 1 - \exp\left(-\frac{t}{\theta}\right) \right\} \exp\left(-\frac{t}{\tau}\right)$$

corresponding to an amplitude

$$V_a = \frac{\bar{q}_{a,s}}{C} \frac{\theta}{\tau}$$

attained at a time $t_m = \tau \ln(\tau/\theta)$, which tends toward zero as θ/τ does.

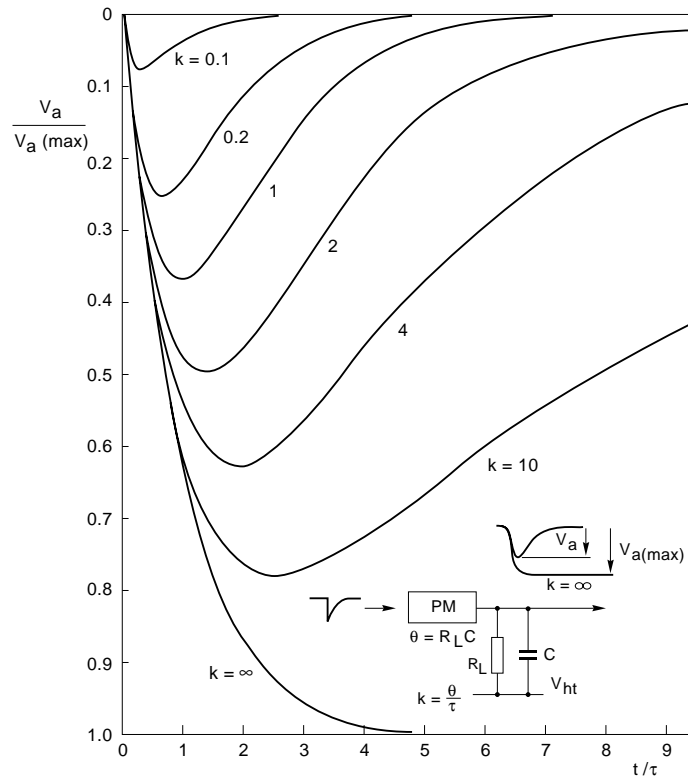


Fig. 6.10 Relative pulse amplitude shapes for an anode load $R_L C$ with $k = \theta/\tau$ as parameter

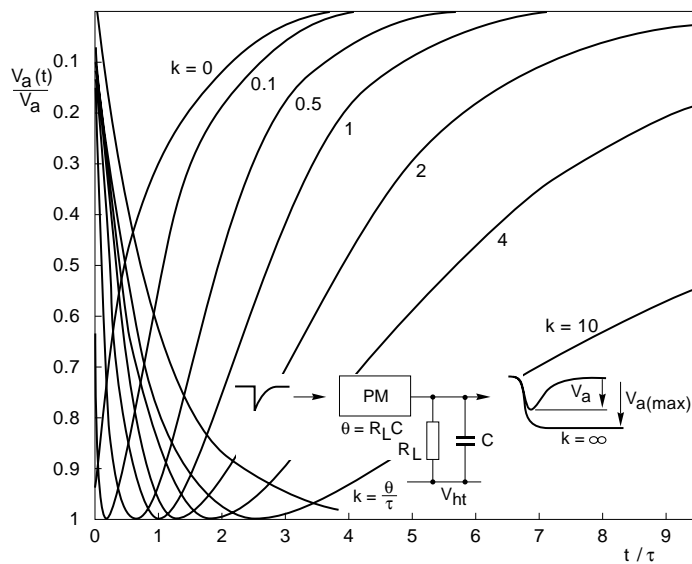


Fig. 6.11 Relative pulse amplitude shapes for an anode load $R_L C$ with $k = \theta/\tau$ as parameter and the amplitudes normalized to 1

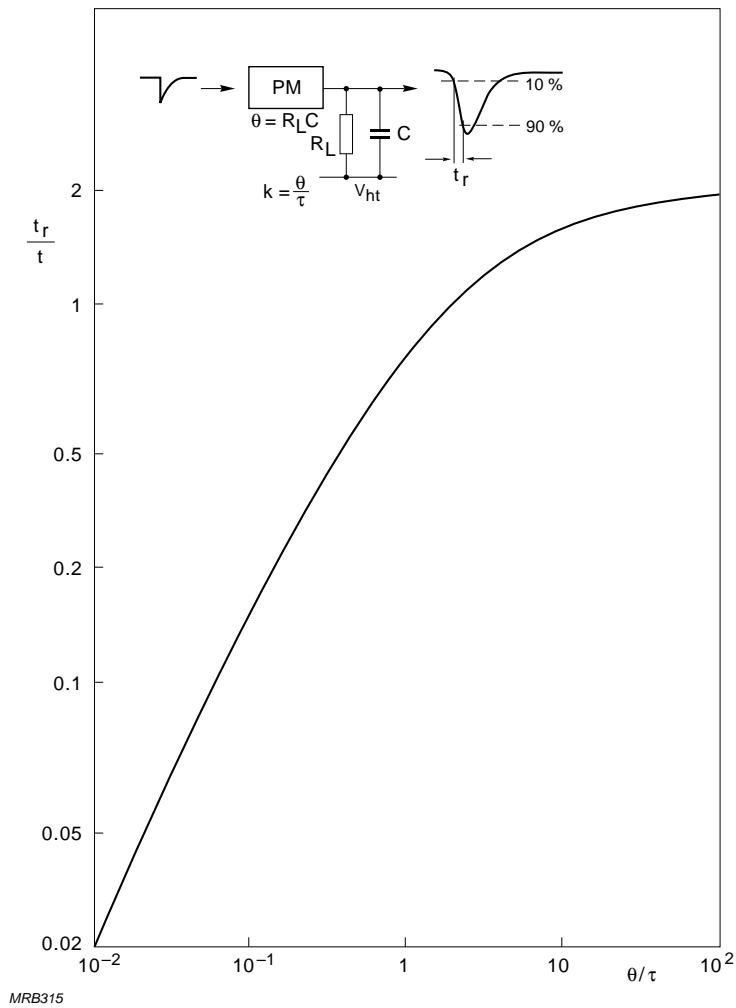


Fig.6.12 Variation of pulse rise time with θ/τ

When $\theta = \tau$, Eq.6.2 reduces to

$$V_a(t) = \frac{\bar{q}_{a,s}}{C} \frac{t}{\tau} \exp\left(-\frac{t}{\tau}\right)$$

corresponding to an amplitude

$$V_a = \frac{\bar{q}_{a,s}}{C} \exp(-1)$$

attained at a time $t_m = \tau$.

When $\theta \gg \tau$, Eq.6.2 approaches the limit

$$V_a(t) = \frac{\bar{q}_{a,s}}{C} \left\{ 1 - \exp\left(-\frac{t}{\tau}\right) \right\} \exp\left(-\frac{t}{\theta}\right)$$

corresponding to an amplitude

$$V_a = \frac{\bar{q}_{a,s}}{C} = V_{a \max}$$

attained at a time $t_m = \tau \ln(\theta/\tau)$, which tends toward infinity as θ/τ does.

Low values of θ/τ allow high count rates and lessen the risk of pulse pile-up, but, because of the larger bandwidth of the circuit, they worsen the signal-to-noise ratio.

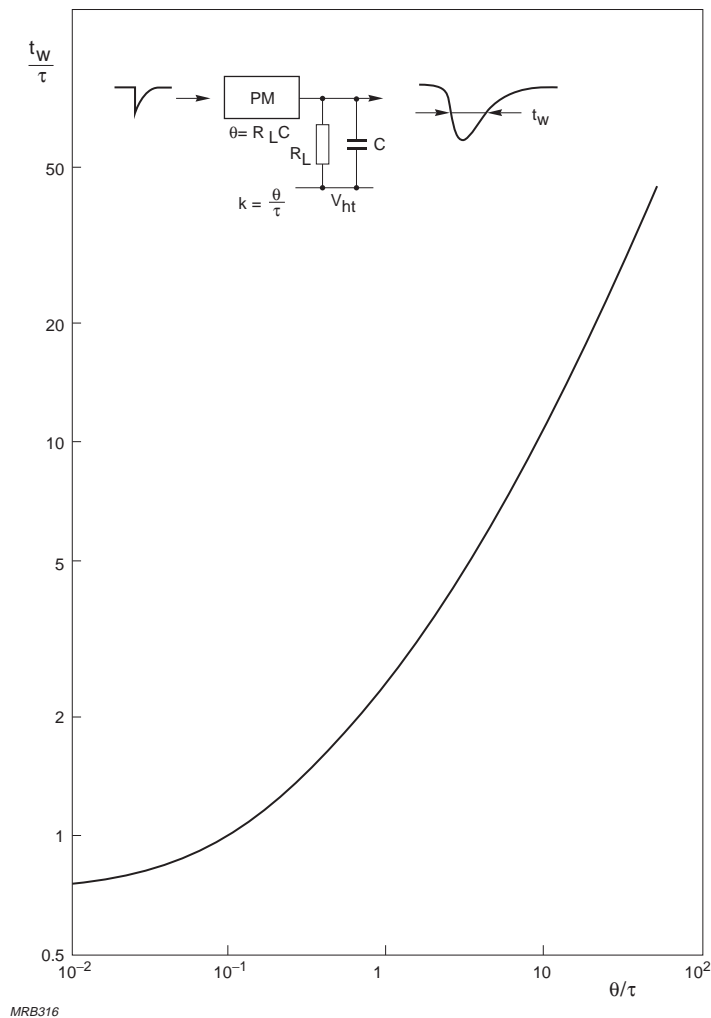


Fig.6.13 Variation of full width at half maximum t_w with θ/τ

6.3 Operating modes

6.3.1 Continuous mode

When a scintillator is used in the continuous mode (as in thickness monitoring, for instance) the photomultiplier anode charges are integrated rather than counted (Fig.6.14). Owing to the quantum nature of radiation and the statistics of energy conversion in the scintillator and photomultiplier, there is therefore some fluctuation of the resulting signal (§3.2.7). The amplitude of this fluctuation depends on the time constant $R_L C$ and the bandwidth of the output electronics or instrument.

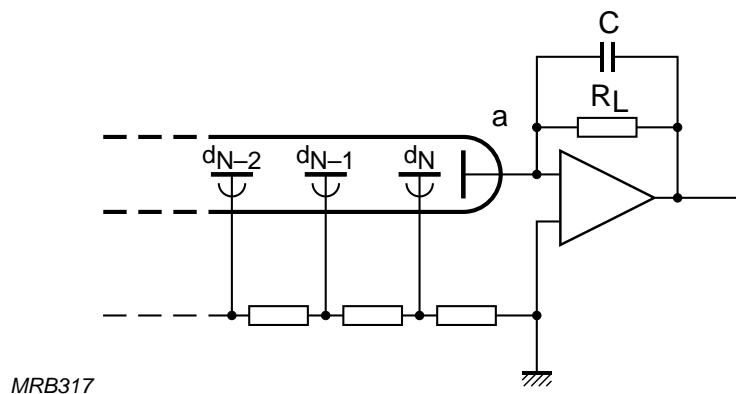


Fig.6.14 Circuit for a photomultiplier in continuous mode

6.3.2 Pulse mode

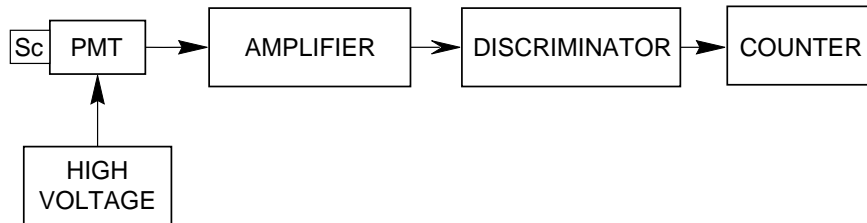
In pulse-mode operation the integration time constant has to be short; how short depends on:

- the pulse characteristics to be measured (amplitude, frequency)
- the pulse characteristics required by the electronics (rise time, duration).

For pulse counting, the time constant is usually made as short possible to be compatible with the high resolution of the detector system. For energy spectrometry it must be long enough to integrate all the charges due to a single event; however, if is too long there is a risk of pulse pile-up. For time spectrometry it is made as short as possible (§5.4.2), often of the same order of magnitude as the transit-time spread of the tube.

Pulse counting

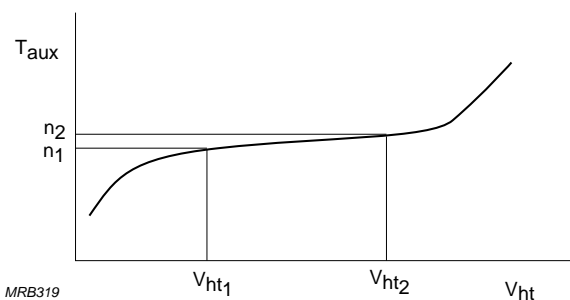
In the set-up illustrated in Fig.6.15 the discriminator selects pulses that exceed a set threshold, or are between a set minimum and maximum (the amplitude window), and passes them to the counter. The pulse frequency registered by the counter is a measure of the radiation intensity to which the scintillator is exposed.



MRB318

Fig.6.15 Block diagram of a scintillator pulse counter

Together, the discriminator threshold and the gain characteristic of the tube define a counting plateau (Fig.6.16) within which the count rate due to a constant radiation flux varies very little as a function of the high voltage applied to the tube. Such a plateau is usually described in terms of its slope (in per cent change of count rate per volt) and its length in volts. Afterpulses, whose rate increases with the applied voltage (§4.7), and dark noise, which is related to field emission, are important factors affecting the slope.



MRB319

Fig.6.16 The discriminator threshold and gain characteristics of the tube define a counting plateau

Resolution time is the least interval between successive scintillations that the counter can distinguish. It is determined either by the decay time constant of the scintillator or the time characteristics of the electronics. With present-day scintillators resolution times of the order of 1 ns can be obtained.

If the dead time of the counter, τ_d , is comparable with the mean interval separating successive scintillations, the counting error may be appreciable. If n_e is the observed count rate, the true count rate corrected for the dead time is

$$n = \frac{n_e}{1 - n_e \tau_d}$$

Environmental effects may increase or decrease the count rate. Background radioactivity increases it. Absorption between the source and the scintillator decreases it. Absorption can be a significant cause of counting error for highly ionizing radiations such as α - and soft β -rays, especially if their free path in the ambient medium is short compared with the distance between source and scintillator. Scatter may increase or decrease the count rate, depending on whether the net deflection of radiation is into or away from the detector.

Statistical considerations also affect counting accuracy. Even when the dead time of the counter is small compared with the mean time interval between scintillations (and environmental effects are negligible), the accuracy of the count is limited by the stochastic nature of the phenomena observed. For example, when measuring radiation intensity (nuclear particles or photons), the measured value of the count rate will have no fixed level but will vary from observation to observation. An estimate of the accuracy of the count rate measured can be made on a statistical basis.

The value of the radiation intensity under observation can be defined as a true mean count rate m taken over an infinite number of observations. The measured count rate is then a variable X whose value x is distributed about m according to a probability distribution appropriate to the phenomena under observation. This distribution will be characterized by the true mean value m and an ideal standard deviation σ_X . Although, when a single observation of X is made, there is no way of knowing whether this is close to m , when N observations x_i of X are made the results can be analysed statistically and an indication of the *probable* accuracy obtained.

First, calculate the experimental mean

$$\bar{x} = \frac{1}{N} \sum_{i=1}^N x_i$$

and the variance about the experimental mean

$$s^2 = \frac{1}{N} \sum_{i=1}^N (x_i - \bar{x})^2$$

The calculated values of both \bar{x} and s^2 will vary from one set of observations to another, and are therefore themselves random variables. They are, however, unbiased estimators of the values m and σ_X required.

When N is large it can be shown that:

- the experimental mean \bar{x} approaches the true mean m
- the value $(\bar{x} - m)$ has a gaussian distribution of variance σ_X^2/N .

Let the mean experimental value be the expectation E of that value, so that the mean value of the experimental variance is $E(s^2)$. Then, with m as the origin of the distribution

$$Ns^2 = \sum_{i=1}^N x_i^2 - N\bar{x}^2$$

The average of N observations is

$$NE(s^2) = NE(x_i^2) - NE(\bar{x}^2) = N\sigma_X^2 - \frac{N\sigma_X^2}{N} = (N - 1)\sigma_X^2$$

and

$$E(s^2) = (N - 1)\frac{\sigma_X^2}{N}$$

Thus, s^2 approaches σ_X^2 as N increases.

Using the gaussian distribution, it is possible to determine the minimum number of observations, N , that must be made so that, with a probability P , \bar{x} is within a given percentage of m . This probability is termed the confidence level of the measurement, Fig.6.17, and is given by $P = (1 - 2\alpha)$, where α is the probability that \bar{x} is further from m by the required amount in any one direction.

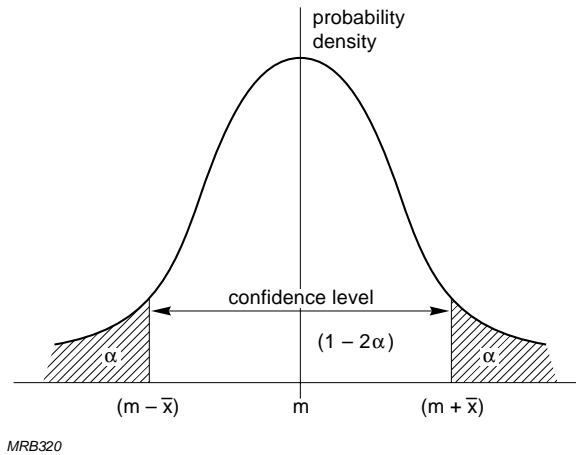


Fig.6.17 The confidence level is the probability that an observation \bar{x} is within a given percentage of the origin m of the distribution

Values of 2α are given in Table 6.1 and plotted in Fig.6.18 for $\kappa\sqrt{N}/\sigma_X$, where the modulo $\kappa = m/(m - \bar{x})$. Thus, to find the number of observations N such that, with a confidence level of 95%, \bar{x} is within 10% of m , read the value of $\kappa\sqrt{N}/\sigma_X$ for $2\alpha = 1 - 0,95 = 0,05$. In Fig.6.18 this is about 2, so, since $\kappa = m/10$

$$\frac{m\sqrt{N}}{10\sigma_X} > 2$$

and

$$N > 400 \left(\frac{\sigma_X}{m} \right)^2$$

Table 6.1 Spot value of 2α

$\kappa\sqrt{N}/\sigma_x$	0.5	0.6745	1	1.349	2	2.024	2.698	3
2α	0.617	0.5	0.317	0.178	0.0455	0.0341	0.00706	0.00272

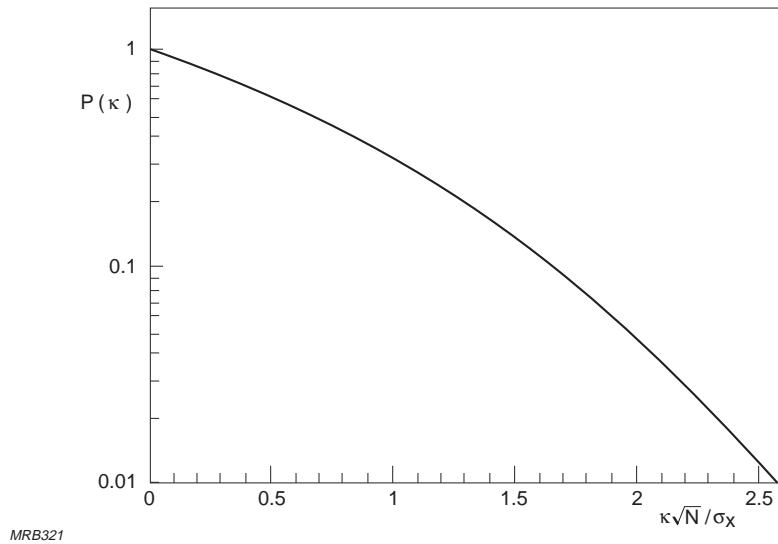
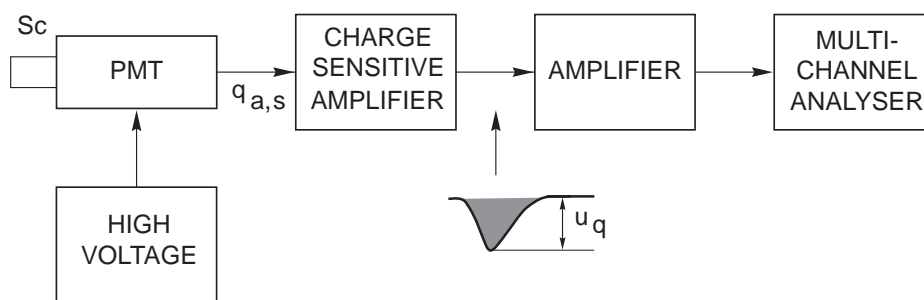


Fig.6.18 Probability $P(\kappa)$ that a variable $(\bar{x} - m)$ is greater than the modulo κ

Energy spectrometry

Figure 6.19 illustrates an energy spectrometer using a multichannel pulse-height analyser. Each interaction in the scintillator gives rise to a photomultiplier anode charge $q_{a,s}$ which is proportional to the energy spent in the interaction. The charge amplifier converts the charge into a proportional voltage pulse u_q which is then amplified and applied to the multichannel analyser. As successive pulses occur the analyser constructs a histogram of their amplitudes.



MRB322

Fig.6.19 Energy spectrometer using a multichannel pulse-height analyser

Energy resolution. For homogeneous (monoenergetic) radiation completely absorbed in the scintillator, the histogram should theoretically consist of a single narrow peak

whose abscissa corresponds to the characteristic energy of the radiation. For non-homogeneous radiation the histogram should consist of a number of such peaks, each with an abscissa corresponding to one energy component of the radiation and a height proportional to the relative frequency of occurrence of that component.

The narrowness of the peaks is a measure of the energy resolution of the scintillator-photomultiplier combination. The following effects always cause some widening of the peaks, and hence loss of resolution:

- Photon emission in the scintillator fluctuates from one monoenergetic interaction to another, mainly because of inhomogeneities in the scintillator and an inherent resolution-degrading component originating from the non-proportionality of the light yield, typical for each scintillator*.
- Photon collection at the cathode fluctuates from one scintillation to another because of variation of the points of origin of successive scintillations, consequent variations of photon path lengths and angles of incidence, and local variations of scintillator window, coupling compound, and cathode window transparency and refractive index.
- Photon-electron conversion efficiency fluctuates because of local variations of cathode sensitivity.
- Electron collection and multiplication fluctuate, mainly because of variations in photoelectron points of origin.

All these cause the voltage pulse u_q to fluctuate from one scintillation to another. If the number of photons emitted per scintillation is large, the pulse height distribution is approximately gaussian, with mean value \bar{u}_q and standard deviation σ_u . From Eq.2.14 the energy resolution R_e is then $\Delta u_q / \bar{u}_q$, where $\Delta u_q = 2.36 \sigma_u$. Or, in terms of the photomultiplier parameters (Eq.3.34),

$$R_e = 2.36 \left(v_{np,s} + \frac{1 - \rho + v_G}{\bar{n}_{p,s} \rho} \right)^{3/2} \quad (6.3)$$

where $\bar{n}_{p,s}$ is proportional to the primary energy E_p absorbed in the scintillator. Equation 6.3 shows that R_e varies inversely as $\sqrt{E_p}$. (The Poisson distribution assumption, $v_{np,s} = 1/\bar{n}_{p,s}$, is, however, not entirely valid, so the resolution is in fact not quite so good as Eq.6.3 would suggest.)

* This is treated in detail in "Inorganic Scintillation Detectors in γ -ray Spectrometry" by M. Moszynski, Elsevier Science, NIM 2002, in print.

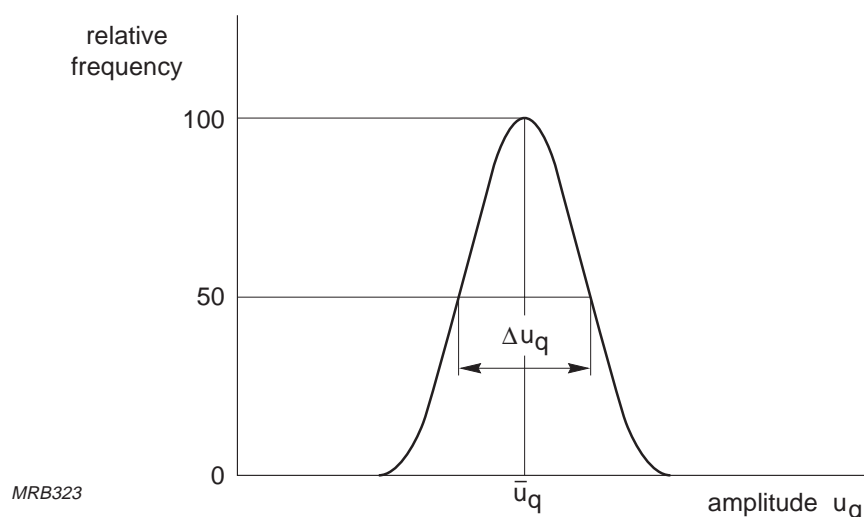


Fig.6.20 Energy resolution $\Delta u_q/u_q$

Energy resolution is measured by taking the FWHM of the full-energy peak (Fig.6.20), dividing it by the energy corresponding to the peak maximum, and multiplying by 100. Commercial diameter 50 mm × 50 mm and diameter 38 mm × 38 mm aluminium encased NaI(Tl) scintillators used in combination with present-day photomultipliers give resolutions of 6–7% for the 662 keV γ -radiation of ^{137}Cs , and 8–9% for the 122 keV γ -radiation of ^{57}Co (Fig.6.21). These are standard sources for such measurements.

A standard source for low-energy measurements is the 5.9 keV X-radiation of ^{55}Fe , and the scintillators usually have a window of beryllium instead of aluminium, for minimum attenuation of the radiation. In the example shown in Fig.6.22 the energy resolution is 30%; the measurement was made using a 32 mm diameter, 2 mm thick NaI(Tl) scintillator with a 36.8 mg/cm² beryllium window.

Another parameter of interest is the peak-to-valley ratio P/V defined as the ratio of the peak value of the amplitude distribution curve to the minimum value of the valley to the left of the peak. The P/V ratio in Fig.6.22 could be estimated as 40:1.

Because electron collection and multiplication in the photomultiplier input stages is a dominant statistical factor in the conversion of incident photon energy to electrical energy, the energy resolution also depends strongly on the voltages applied to those stages. Figure 6.23 shows examples of energy resolution variation as a function of cathode to first-dynode voltage obtained with three radiation sources: ^{55}Fe , ^{57}Co , and ^{137}Cs . From these it is apparent that energy resolution is best when the cathode to first dynode voltage is between about 200 V and 300 V.

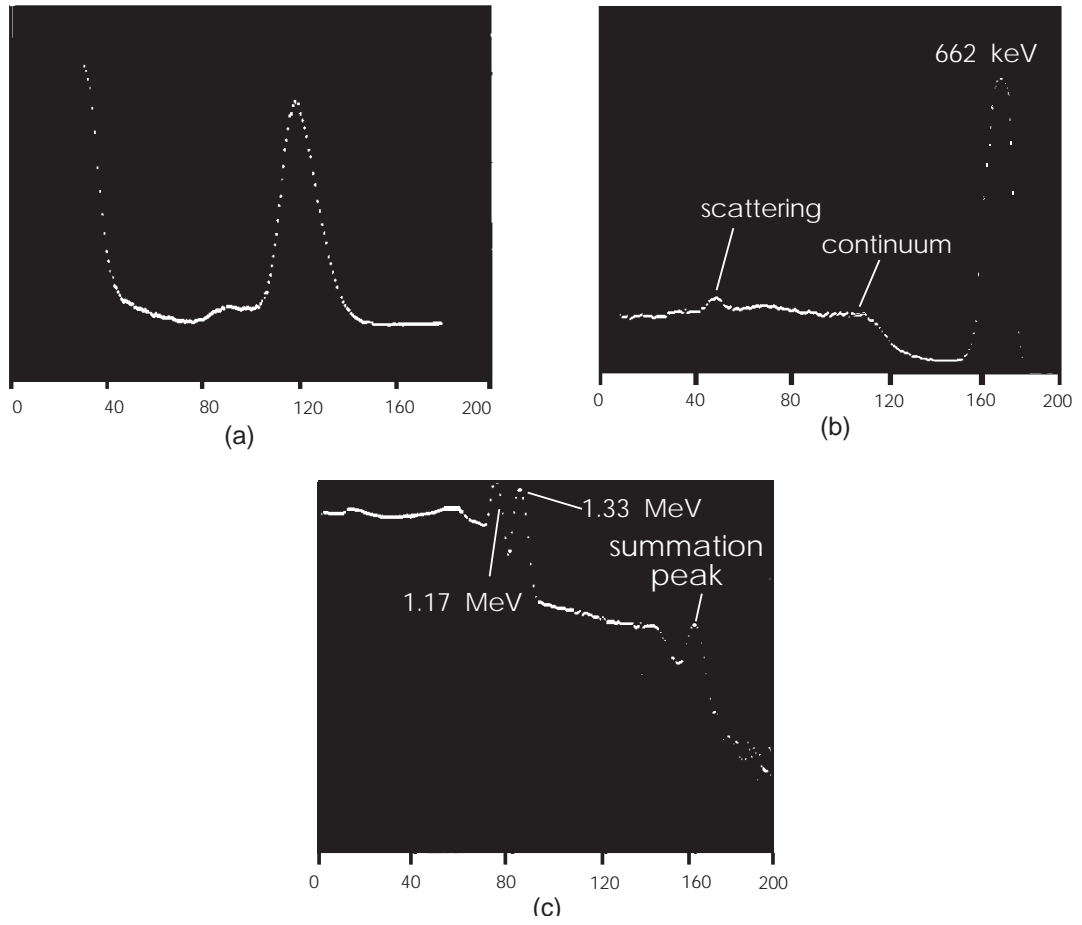


Fig.6.21 Scintillator pulse amplitude distribution using sources of (a) ^{57}Co , (b) ^{137}Cs and (c) ^{60}Co

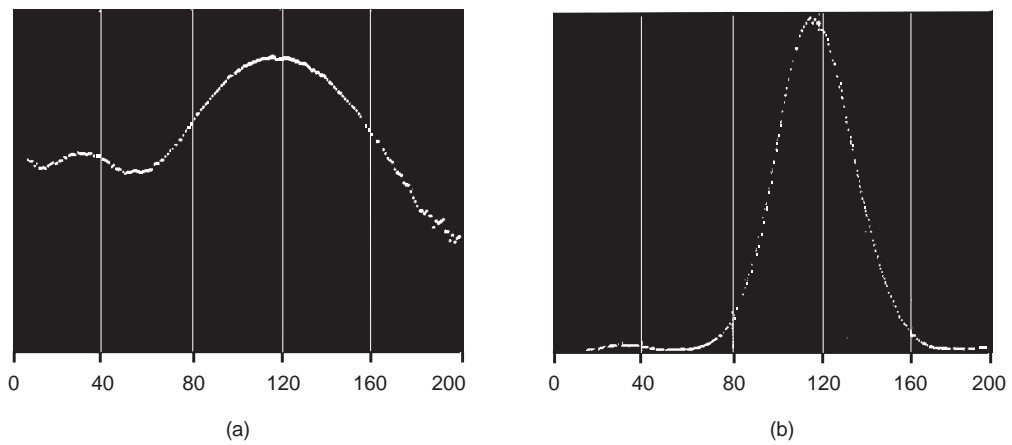


Fig.6.22 Scintillation pulse amplitude distribution for a ^{55}Fe source with (a) a logarithmic and (b) a linear scale on the y axis

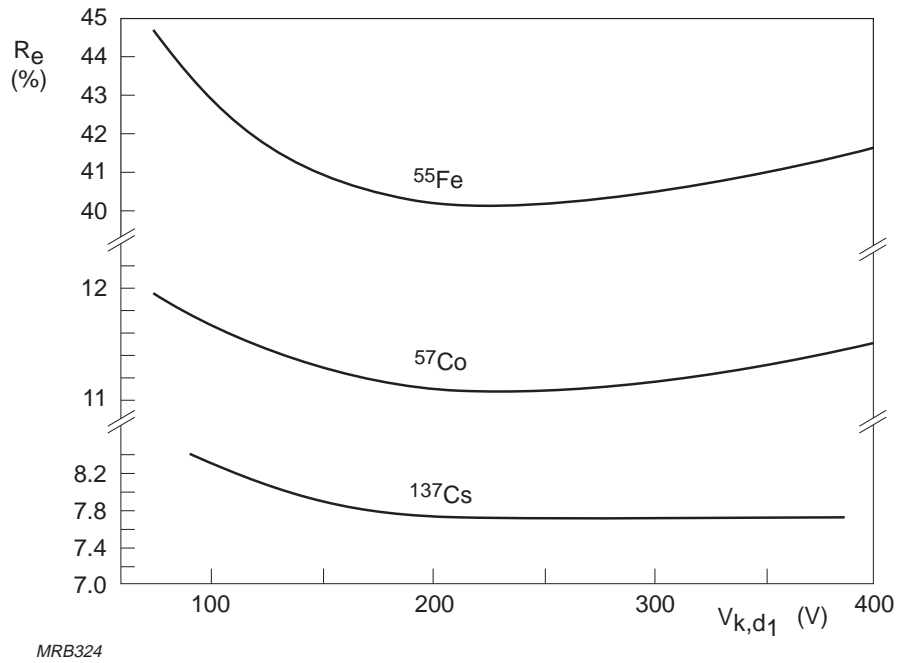


Fig.6.23 Energy resolution variation as a function of cathode to first-dynode voltage. Sources ^{55}Fe , ^{57}Co and ^{137}Cs

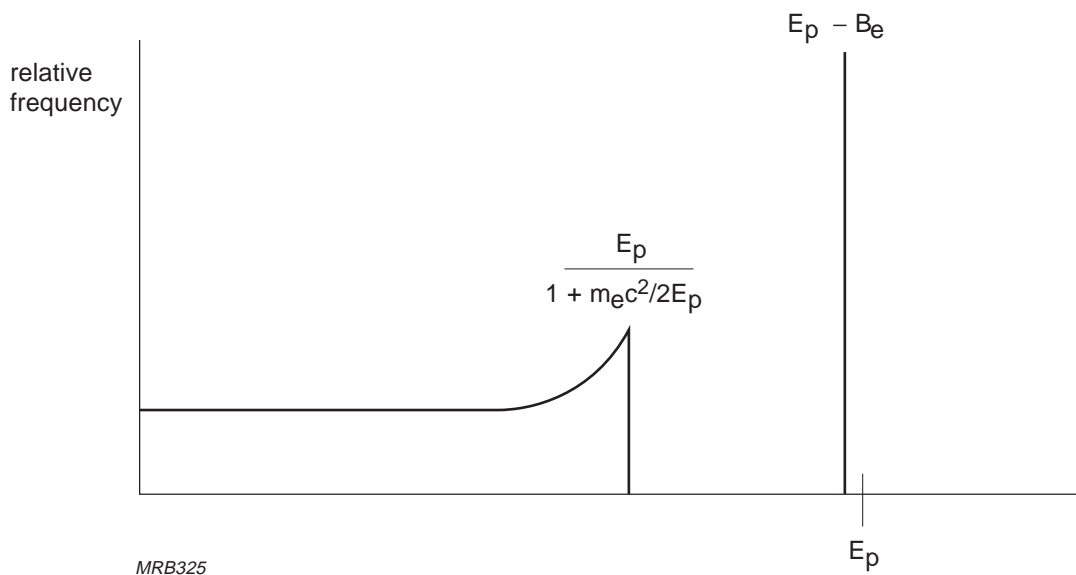


Fig.6.24 Spectrum of primary electron energies produced in a scintillator by monoenergetic γ radiation of energy E_p , showing the Compton continuum, the Compton edge and the photoelectric line

Composition of the pulse-height spectrum. The proportionality between the primary energy E_p absorbed in the scintillator and the mean number of photons received at the cathode, $\bar{n}_{p,s}$, depends on the interaction processes by which radiation absorbed in the scintillator liberates electrons and thereby excites fluorescence (see Appendix to this chapter). If there were but one such process, the pulse-height spectrum due to a monoenergetic source of X- or γ -radiation would consist of a single peak – the ‘full energy peak’ – corresponding to the energy E_p .

In reality, however, the composition of the spectrum is not that simple (Fig.6.24). There are not one but three primary processes by which radiation is absorbed, each of which leaves its own signature on the spectrum. Moreover, there are various secondary phenomena which also play a part. The three primary processes are: photoelectric effect, Compton effect, and pair production. Each of these liberates electrons of a characteristic energy E_s which excite fluorescence of a corresponding intensity.

– *Photoelectric effect:* $E_{s,p} = E_p - B_e$

Here, B_e is the binding energy of the liberated electron, which is usually ejected from a K or L shell. When the vacancy left by its ejection is again filled, the energy B_e reappears as characteristic X-rays and Auger electrons. If these occur within the response time for the primary photoelectric event, the fluorescence they excite also contributes to the photo-peak corresponding to that event. In that case, the photo-peak becomes equivalent to a full-energy peak E_p .

– *Compton effect:* $0 \leq E_{s,c} \leq E_p/(1 + m_e c^2/2E_p)$

where m_e is the rest mass of the electron and c the free-space velocity of light ($m_e c^2 = 0.511$ MeV). Besides the primary electron of energy $E_{s,c}$, a Compton interaction yields a secondary photon of energy

$$E'_p = \frac{E_p}{1 + (1 - \cos\theta)\frac{E_p}{m_e c^2}}$$

where θ is the angle between the path of the secondary photon and the original X- or γ -photon. If the secondary photon is absorbed within the scintillator, the Compton interaction contributes to the full-energy peak. Otherwise, it yields a continuous spectrum (the ‘Compton continuum’) extending from zero up to the energy $E_p/(1 + m_e c^2/2E_p)$, which corresponds to a spectral feature known as the ‘Compton edge’.

- *Pair production*: $E_{s,pp} = E_p - 2m_e c^2$
 where $2m_e c^2$ represents the rest-mass energy of an electron-positron pair created by the absorption of a γ -photon. The contribution of pair-production events to the spectrum depends on whether both, one, or neither of the photons due to subsequent annihilation of the positron escapes from the scintillator without further interaction. If both escape, the pair-production event contributes to a spectral peak at $E_p - 1.02$ MeV, which is usually superimposed on the Compton continuum. If only one escapes, the event contributes to a peak at $E_p - 0.511$ MeV. And if neither escapes, it contributes to the full-energy peak E_p . All three of these possibilities may appear in a single spectrum.

Secondary effects that may influence the shape of the pulse-height spectrum include X-escape, back-scatter, annihilation, and sum peaks:

- *X-escape peak*. If an X-photon due to a photoelectric interaction escapes from the scintillator, the scintillation energy for that interaction will be correspondingly diminished. In an NaI(Tl) scintillator the loss amounts to some 28 keV. In the spectra of low-energy radiation sources this gives a secondary peak 28 keV to the left of the photo-peak. In higher-energy spectra the X-escape peak is so close to the photo-peak that it is indistinguishable.
- *Back-scatter peak*. Compton effect interactions can scatter low-energy photons back into the scintillator from the surroundings. These may produce an observable photo-peak in the Compton continuum, usually centred at an energy slightly greater than $E_p / (1 + 2E_p / m_e c^2)$.
- *Annihilation peak*. Pair-production interactions in the immediate surroundings (or in the radiation source itself) may scatter annihilation photons into the scintillator. These produce a spectral peak at 0.511 MeV.
- *Sum peaks*. Sources that emit γ -radiation of two distinct energies, E_{p1} and E_{p2} , produce a spectrum with two corresponding full-energy peaks. However, when the two radiations are emitted simultaneously within the response time of the scintillator-photomultiplier combination, they produce a third spectral peak corresponding to $E_{p1} + E_{p2}$. Examples of sources that produce such peaks are ^{60}Co (see Fig.6.21(c)) and ^{24}Na . The latter produces a sum peak corresponding to its 1.274 MeV γ -radiation plus the 0.511 MeV due to annihilation of a pair-production positron.

In general, the larger the scintillator, the more prominent is the full-energy peak relative to such features as the Compton continuum and pair-production, back-scatter and X-escape peaks. This is illustrated by Fig.6.25 in which comparable spectra obtained with three sizes of scintillator have been normalized with respect to the area under the full-energy peak. The fraction of the total recorded pulses that appears under the full-energy peak is called the photoelectric efficiency, ϵ_{ph} , of the scintillator.

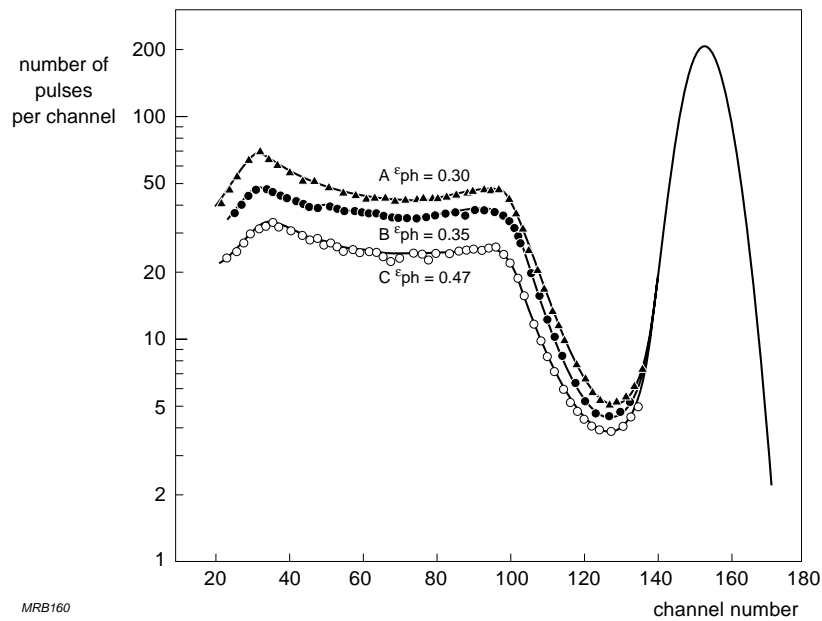


Fig.6.25 Scintillation pulse amplitude distributions with ^{137}Cs sources and scintillators of dimensions $\phi 38 \text{ mm} \times 25 \text{ mm}$ (A), $\phi 50 \text{ mm} \times 50 \text{ mm}$ (B) and $\phi 75 \text{ mm} \times 75 \text{ mm}$ (C). The distributions are normalized to give the same area under their full energy peak curves

Time spectrometry

Time spectrometry is used to measure time relations between events such as the emission of particles or photons in cascade or the de-excitation of nuclear states. It requires fast-response photomultipliers and fast-response scintillators with high scintillation effectiveness (Appendix A6.3).

The time spectrometry principle can also be used to measure scintillator response time, as in the set-up shown in Fig.6.26. Here, the two γ -photons emitted in cascade by a ^{60}Co source provide the basis for measurement. Pulses from the two photomultipliers are amplified, shaped, and applied via discriminators to a time-to-pulse-height converter. A multichannel analyser at its output generates a distribution plot (Fig.6.27) of the time differences measured for each pulse pair.

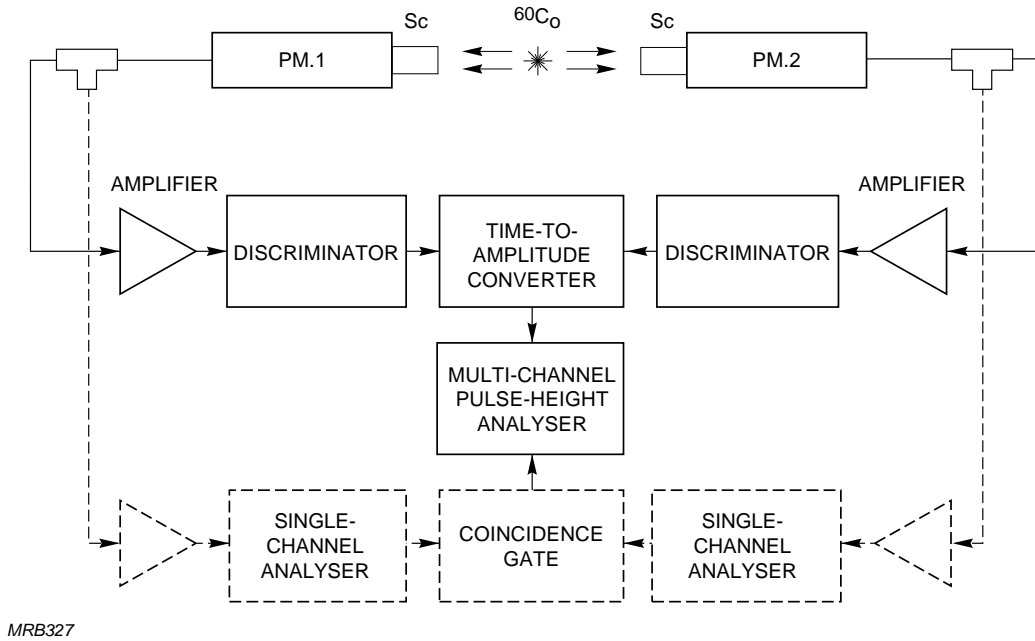


Fig.6.26 Basic setup for time spectrometry

To minimize errors due to photomultiplier pulse amplitude fluctuations ('walk errors'), the parallel channel shown dotted in Fig.6.26 gates the multichannel analyser to accept time-proportional pulses only when the corresponding photomultiplier pulses occupy a set amplitude window. Walk errors can be further reduced by using discriminators in the main channel that trigger at an optimum point on the pulse leading edges regardless of peak pulse amplitude ('constant fraction triggering').

With respect to the instant of γ -photon emission, the response-time variance of either of the two detectors is, from Eq.4.18

$$\sigma_t^{*2} = \frac{\tau^2 + \sigma_t^2}{\bar{n}_{k,s}}$$

where τ is the scintillation decay time constant, σ_t the standard deviation of the photomultiplier transit time fluctuations, and $\bar{n}_{k,s}$ the mean number of photoelectrons emitted at the photocathode per scintillation. If the statistics are gaussian, the variance of the two detectors together can be obtained by summing the individual variances; thus,

$$\sigma_{t,t}^{*2} = 2 \frac{\tau^2 + \sigma_t^2}{\bar{n}_{k,s}}$$

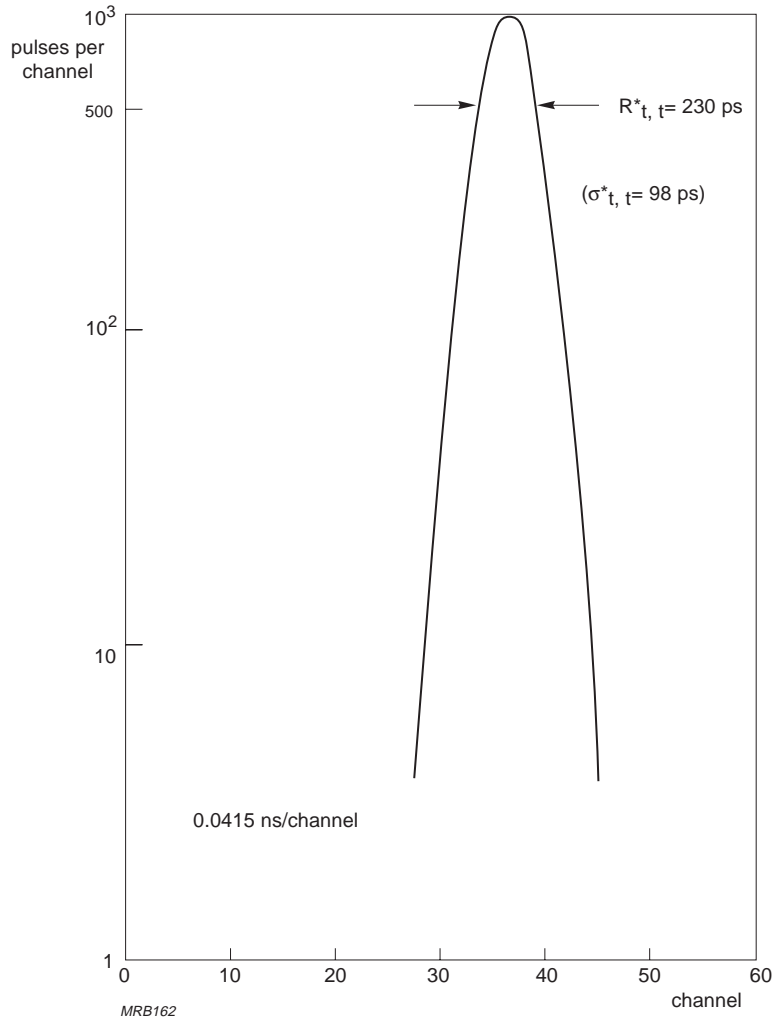


Fig.6.27 Coincidence time resolution distribution from two fast scintillation counters for ^{60}Co coincidence γ - γ radiation

The lowest values of τ for fast-decay plastic scintillators are a few nanoseconds, whereas the lowest values of σ_t for fast-response photomultipliers are only a few tenths of a nanosecond. The greater part of the response time variance is therefore due to the scintillator.

The spectrometer time resolution $R_{t,t}^*$ is defined as the FWHM of the observed response-time distribution,

$$R_{t,t}^* = 2.36 \sigma_{t,t}^*$$

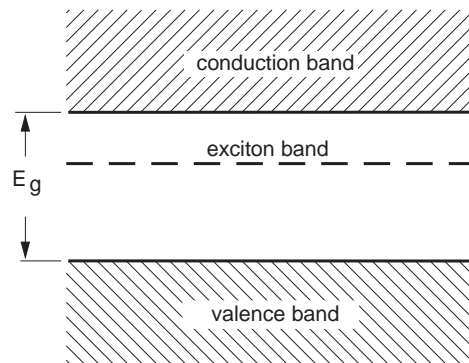
Since $\sigma_{t,t}^*$ varies inversely as the square root of the mean number of photoelectrons excited per scintillation, $\sqrt{\bar{n}_{k,s}}$, it is obvious that the choice of an efficient scintillator is very important in time spectrometry. Using very fast response photomultipliers and the fastest plastic scintillators (or BaF_2) for which $\tau < 3$ ns, values of $R_{t,t}^* < 200$ ps can be obtained.

APPENDIX 6 SCINTILLATOR FUNDAMENTALS

Scintillators are substances which convert some of the energy of incident radiation into detectable photons. They fall into two main classes, inorganic and organic, which differ not only chemically but also in the processes by which they release photons.

A6.1 Inorganic scintillators

Luminescence in inorganic scintillators is mainly a crystal property; it does not occur in liquids or gases, except in some inert gases in which it is an atomic or molecular property. Inorganic scintillators are crystalline compounds in which luminescence originates from emission centres in the compounds themselves or formed by activating agents introduced in controlled amounts (§A6.4).



MRB329

Fig.A6.1 Energy band diagram in an inorganic crystal

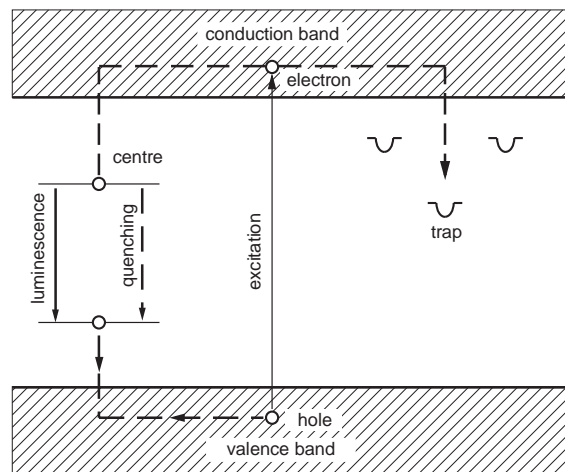
Scintillator crystals are usually insulators or semiconductors having an energy gap of a few electron volts between the valence and conduction bands (Fig.A6.1). Under the influence of ionizing radiation, electrons in the valence band can acquire sufficient energy to reach the conduction band, leaving behind charge deficiencies (positive 'holes') in the valence band. The crystal is then ionized and photoconductive. If the energy imparted to an electron is insufficient to raise it to the conduction band, it remains bound to a hole, at an energy level just below the conduction band. The electron-hole pair is called an 'exciton'.

This description applies only to a perfect crystal. Imperfections due to lattice dislocations or impurities in the crystal create additional energy levels in the energy gap into which excitons in the gap or electrons in the conduction band can move (Fig.A6.2). These levels correspond to activation centres of three types:

Luminescence centres, at which recombination of an electron-hole pair brings the centre to an excited state from which it returns to the ground state by photon emission; this is called fluorescence. The electron-hole recombination that excites the centre can be due either to capture or an exciton or to simultaneous capture of an electron from the conduction band and a hole from the valence band.

Quenching centres, which are like luminescence centres except that the excitation energy is dissipated as heat (phonons) instead of light.

Traps, which are metastable levels at which electrons and holes, or excitons, can remain for a long time before acquiring sufficient thermal energy to return to the conduction and valence bands or to move to a luminescence or quenching centre. When they do move to a luminescence centre the delayed emission that results is called phosphorescence.



MRB330

Fig.A6.2 Discrete levels within the forbidden band caused by crystal impurities

A6.2 Organic scintillators

Luminescence in organic substances is a molecular phenomenon which can occur in the solid, liquid or vapour phase as well as in liquid or solid solutions and plastic and glassy states.

Organic compounds form molecular crystals in which the occurrence of luminescence is associated with transitions between different energy levels of the electron systems: the singlet levels S_0, S_1, \dots, S_n ; and the triplet levels T_1, T_2, \dots, T_n (Fig.A6.3).

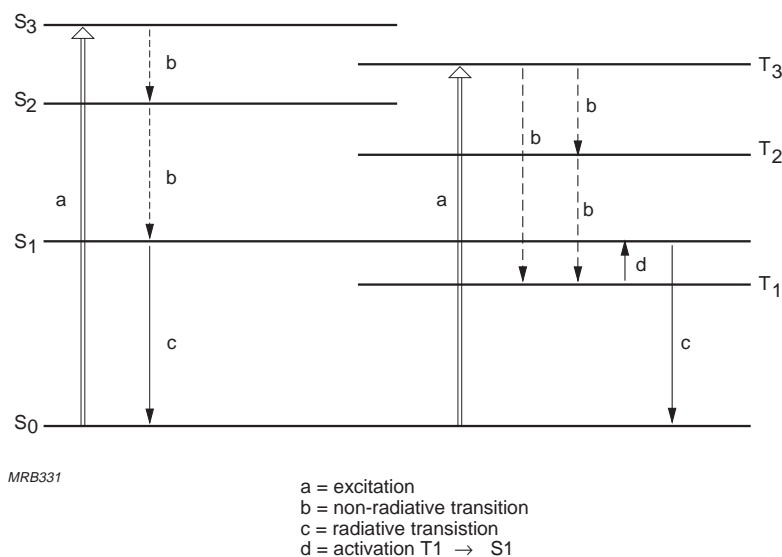


Fig.A6.3 In organic compounds, luminescence is associated with electron transitions between different energy levels (singlet and triplet states)

In the ground state the electrons are at the S_0 level. Incident radiation can either excite a molecule, raising its system of π electrons to a high singlet level (S_n), or ionize it, forming a free electron and a positive ion. Fast recombination of the electron and ion produces an excited molecule at a triplet level T_n or, less probably, a singlet level S_n . Non-radiative internal conversion phenomena then quickly return the excited levels to the lowest triplet or singlet levels, T_1 or S_1 ; these phenomena take about 10 to 100 ps.

The S_1 excited state, which lasts for about a nanosecond, can return to the ground state S_0 by either of two processes: thermal degradation (inhibition) or photon emission. The latter is called prompt fluorescence.

The T_1 excited state lasts much longer, and the molecule may return from it to the ground state by either of two routes. A direct return from T_1 to S_0 with photon emission is called phosphorescence. The emission is at a longer wavelength than fluorescence and the decay, which is exponential, is also longer – sometimes approaching a millisecond. Alternatively, interaction between two molecules in excited triplet states may raise one of them from the T_1 to the S_1 state, from which it can then return to the ground state; as before either by thermal degradation or by photon emission. In this case the emission is of the same wavelength as fluorescence but the decay is non-exponential.

A6.3 Scintillator characteristics

Scintillators are usually characterized in terms of scintillation effectiveness, scintillation efficiency, emission spectrum, integral quantum efficiency and response time.

Scintillation effectiveness ϵ_s is the ratio of the number of photons emitted per unit time, n_p , to the energy of the radiation absorbed in the scintillator, E_a ,

$$\epsilon_s = \frac{n_p}{E_a}$$

usually expressed in photons per MeV.

Scintillation efficiency η_s is the product of scintillation effectiveness ϵ_s and the energy $h\nu$ of the emitted photons,

$$\eta_s = \epsilon_s h\nu = \frac{n_p h\nu}{E_a}$$

usually expressed as a percentage.

An important consideration in energy spectrometry and a phenomenon that is often forgotten is scintillator linearity. This is a measure of the energy range over which scintillation effectiveness and scintillation efficiency are constant; this range is usually not too wide.

Emission spectrum is characterized by two parameters:

λ_m , the wavelength of maximum emission

$\Delta\lambda$, the FWHM of the emission band.

A useful measure of the spectral matching between a specific scintillator and a specific photomultiplier is the matching factor F_m :

$$F_m = \frac{\int_0^{\infty} R_{e,\lambda} \Phi_{e,\lambda} d\lambda}{\int_0^{\infty} \Phi_{e,\lambda} d\lambda}$$

where $\Phi_{e,\lambda}$ is the spectral distribution of the scintillator emission and $R_{e,\lambda}$ is the relative spectral sensitivity characteristic of the photomultiplier,

$$R_{e,\lambda} = \frac{S_{a,\lambda}}{S_m}$$

where $S_{a,\lambda}$ is as defined by Eq.2.9b and S_m is the sensitivity corresponding to the maximum of $S_{a,\lambda}$.

The matching factor F_m corresponds to the area ratio A_1/A_2 in Fig.A6.4. Table A6.1 lists the matching factors between some photocathodes and 2856 K tungsten light.

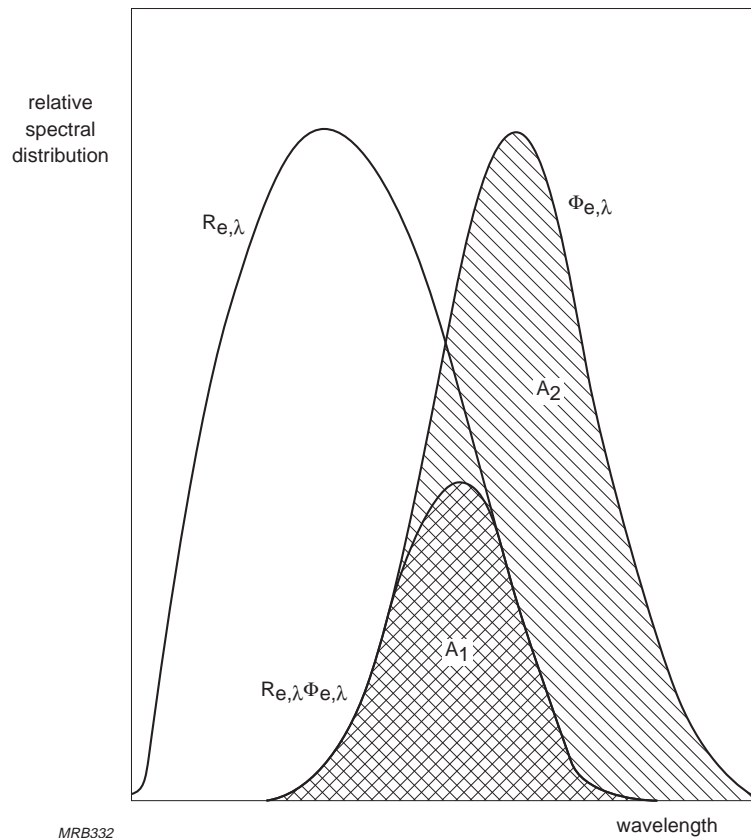


Fig.A6.4 Definition of matching factor $F_M = A_1/A_2$

Table A6.1 Matching factors between several photocathodes and 2856 K tungsten light

type of photocathode	S11 S13	bialkaline	S4	S20	S20R	S1
matching factor F_m	0.028	0.018	0.021	0.056	0.126	0.251

Integral Quantum Efficiency, IQE is defined for a non-monochromatic radiation as the ratio of the average number of emitted photoelectrons to the average number of received photons whatever their energy is.

$$\text{IQE} = \frac{hc}{e} \frac{\int_0^{\infty} S_{a,\lambda} \Phi_{e,\lambda} d\lambda}{\int_0^{\infty} \Phi_{e,\lambda} \lambda d\lambda}$$

with $e = 1.6 \times 10^{-19} \text{ C}$
 $h = \text{Planck's constant}$
 $c = \text{speed of light in vacuum.}$

For the wavelength shifters BBQ, Y7 and K27, typical IQE values are:

Type of photocathode	IQE
monoalkaline S11 SbKCs ₃	10-15%
bialkaline SbKCs	10-15%
green-extended bialkaline (GEBA) SbKCs	12-18%
trialkaline S20 SbNa ₂ KCs	15-22%

Response time is a measure of the width of the scintillator pulse, which is usually much greater than the stopping time of the ionizing particle or photon that causes it. After rising abruptly, the pulse falls according to a composite law in which at least two components can usually be distinguished:

- a fast exponential decay (fluorescence) with a time constant τ
- a slower decay (phosphorescence, delayed fluorescence) following a more complex law.

The time constant τ is called the response of the scintillator.

A6.4 Scintillator properties

A6.4.1 Inorganic-scintillator properties

Except for the inert gases and some specially formulated glasses, inorganic scintillators are either monocrystals or polycrystalline powders. The monocrystals are transparent to their own luminescence, the polycrystalline powers are less so.

The principle monocrystalline scintillators are alkali halides, mostly doped with heavy metals such as thallium or europium: NaI(Tl), CsI(Tl), CsI(Na), KI(Tl), CaI₂(Eu), and CaF₂(Eu). Crystals of pure (undoped) alkali halides like NaI and CsI are also very useful.

Other, more recently adopted monocrystalline scintillators are CaWO_4 , CdWO_4 , PbWO_4 , ZnWO_4 , BaF_2 , CsF , CeF_3 , $\text{Bi}_4\text{Ge}_3\text{O}_{12}$ (colloquially, BGO), and the Ce-doped $\text{Gd}_2\text{SiO}_5:\text{Ce}$ (gadolinium orthosilicate or GSO), Lu_2SiO_5 (lutetium orthosilicate or LSO), $\text{Y}_2\text{SiO}_5:\text{Ce}$ (yttrium orthosilicate or YSO) and $\text{YAlO}_3:\text{Ce}$ (yttrium aluminium perovskite or YAP).

Table A6.2 Properties of some inorganic scintillators

scintillator composition	density (g/cm^3)	index of refraction	wavelength of maximum emission (nm)	decay time constant 1/e (ns)	scintillation pulse height ¹⁾	notes
NaI	3.67	1.78	303	60	190	2)
NaI(Tl)	3.67	1.85	410	250	100	3)
CsI	4.51	1.95	310	10	6	3)
CsI(Tl)	4.51	1.79	565	1000	45	3)
CsI(Na)	4.51	1.84	420	630	85	3)
⁶ LiI(Eu)	4.06	1.96	470-485	1400	35	3)
$\text{CaF}_2(\text{Eu})$	3.19	1.44	435	900	50	
BaF_2	4.88	1.49	190/220 310	0.6 630	5 15	
BGO	7.13	2.15	480	300	10	
ZnWO_4	7.87	2.2	480	5000	26	
CdWO_4	7.90	2.3	540	5000	40	
PbWO_4	8.28	2.16	480	2/7/26	0.8	
CsF	4.65	1.48	390	5	5	3)
CeF_3	6.16	1.68	300 340	5 20	5	
LSO	7.40	1.81	420	42	75	
GSO	6.71	1.9	440	60	20	
YSO	4.45	1.8	420	35	50	
YAP	5.50	1.9	370	30	40	
$\text{ZnS}(\text{Ag})$	4.09	2.35	450	200	150	4)
$\text{ZnO}(\text{Ga})$	5.61	2.02	385	0.4	40	4)

¹⁾ relative to NaI(Tl) ²⁾ at 80 K ³⁾ hygroscopic ⁴⁾ polycrystalline

Polycrystalline powders include the doped sulphides $\text{ZnS}(\text{Cu})$, $\text{ZnS}(\text{Ag})$ and $\text{CdS}(\text{Ag})$, $\text{ZnO}(\text{Ga})$, and the oxide ZnO . NaI(Tl) is also sometimes used as a polycrystalline powder. Being partly opaque to their own luminescence, polycrystalline powders are

mostly used as thin screens which detect only heavy and highly ionizing particles with good efficiency.

Table A6.2 summarizes the properties of some principal inorganic scintillators. In general they have the following properties in common:

- high absorption for X- and γ -photons and nuclear particles such as α and β
- good matching with the spectral sensitivity of general-purpose photomultipliers
- practically linear scintillation effectiveness over a wide energy range
- decay time constants mostly in the region of a microsecond or less.

The list of inorganic scintillators grows yearly, and investigators worldwide are currently devoting a lot of effort to the search for new heavy, non-hygroscopic scintillator materials that are also inexpensive to produce. Interest is presently centred on the fluorides (e.g. ThF_4 , BaLiF_3 , LiYbF_4 , BaYb_2F_4 and PbF_2). Applications for new materials will increase in the coming years, notably in high-energy physics experiments. For the CERN CMS experiment at the Large Hadron Collider (LHC), considerable effort in cooperation with Russian and Chinese centres have gone into the development of the new PbWO_4 scintillator. In nuclear medical imaging, especially for the strongly growing market of PET scanners (Chapter 7), considerable effort is being devoted to finding heavier and faster inorganic scintillators than the fairly new and currently preferred LSO which is gradually replacing the traditional BGO.

Radiation absorption. Because of their high density (3 to 4 g/cm^3) and the high atomic number of iodine ($Z = 53$), monocrystals of the alkali iodides are particularly well suited for detecting X- and γ -photons; see Fig.A6.5. They are also highly absorbent for electrons and heavy charged particles (α , protons, etc.); see Fig.A6.6 and A6.7.

The large neutron cross-section of ${}^6\text{Li}$ makes ${}^6\text{LiI}(\text{Eu})$ an efficient neutron detector. Mixtures of ZnS with ${}^6\text{Li}$, ${}^{10}\text{B}$, ${}^{235}\text{U}$, or even methyl methacrylate, make excellent detectors for thermal neutrons.

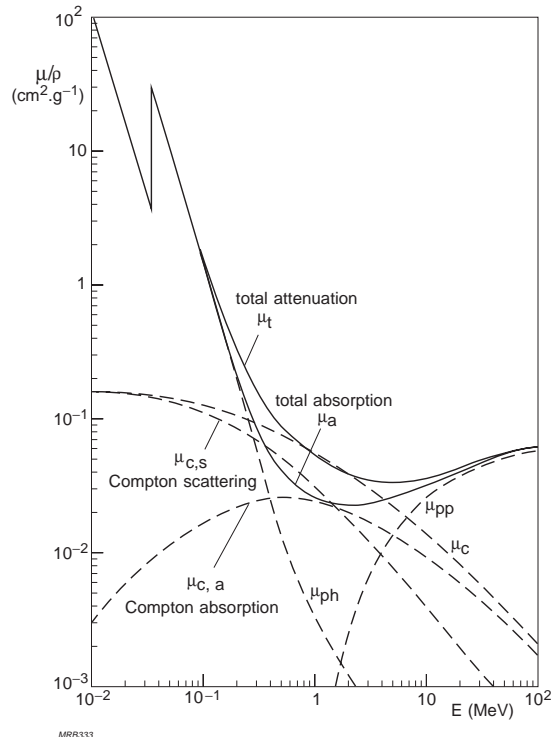


Fig.A6.5 Mass attenuation and mass absorption coefficients for X- and γ -radiation in NaI(Tl), $\rho = 3,67 \text{ g/cm}^3$

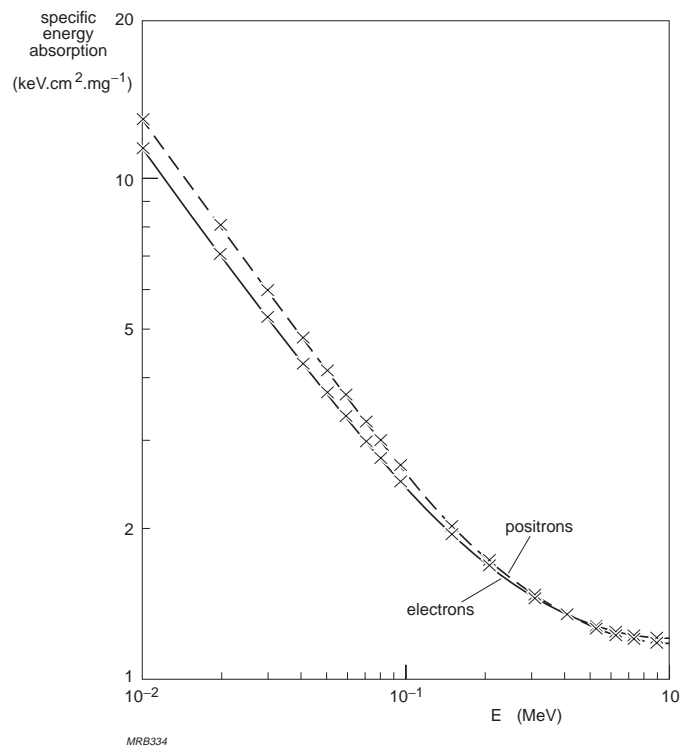


Fig.A6.6 Specific energy absorption for electrons and positrons in pure NaI as a function of their energy (*U.S. National of Bureau Standards, circular number 577, 1956*)

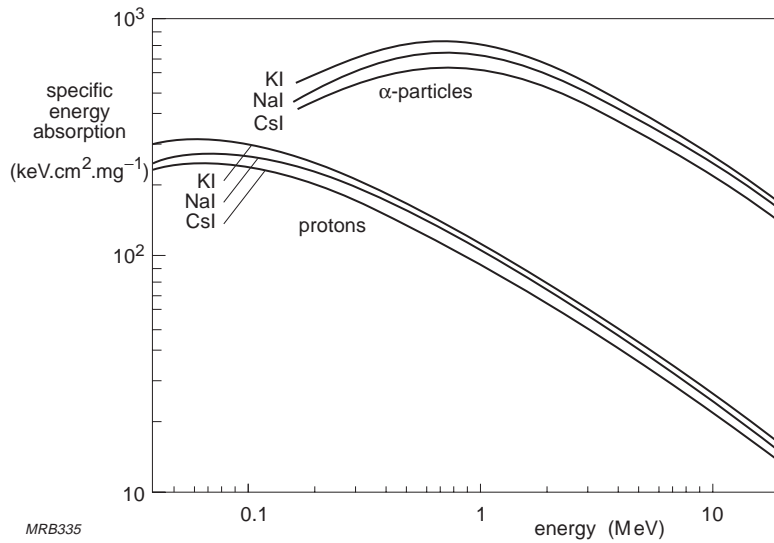


Fig.A6.7 Specific energy absorption for ionizing α -particles and protons in pure KI, NaI and CsI scintillators

Emission spectrum. Inorganic scintillators usually have two emission bands: one due to the activator and another, at shorter wavelength, due to the crystal lattice (see entries for doped and undoped NaI and CsI in Table A6.2). The relative intensity of the emission due to the crystal lattice decreases as the concentration of the activator increases; at high enough concentrations (e.g. 0.1% to 0.5% Tl in NaI) only the emission due to the activator is practically significant. Figure A6.8 compares the emission spectra of Tl-doped NaI ($\lambda_m = 410$ nm) and the undoped scintillator $\text{Bi}_4\text{Ge}_3\text{O}_{12}$ ($\lambda_m = 480$ nm).

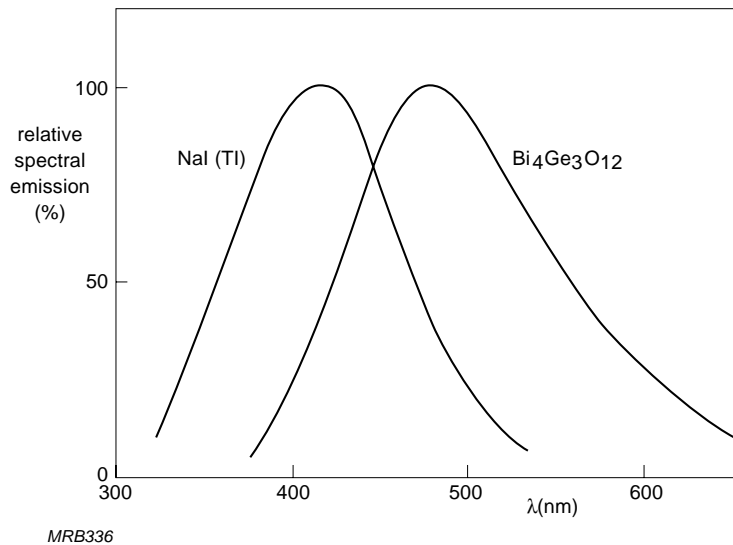


Fig.A6.8 Normalized emission spectra of NaI(Tl) and $\text{Bi}_4\text{Ge}_3\text{O}_{12}$

Scintillation efficiency. The efficiency of most scintillators used in radiation spectrometry can be taken as constant over a wide range; however, a 15% to 20% increase of efficiency at the low-energy end of the range is often observed.

Of the monocrystalline scintillators, the efficiencies of NaI and CsI are among the highest known. NaI(Tl) has an efficiency of about 13%, emitting four or five photons or 3 eV average energy per 100 eV of absorbed energy.

ZnS has higher efficiency than any monocrystalline scintillator. ZnS(Ag) and ZnS(Cu) have efficiencies of about 25% and 30% for α -particles, regardless of the energy of the particles, and about half that for β -particles.

The efficiency of most scintillators as particle detectors varies according to the type of particle being detected. NaI(Tl) is most efficient for protons and deuterons and progressively less so for electrons, α -particles, and heavy ions.

Response time. The shape of the scintillation pulse depends on factors such as the type of crystal, the nature and concentration of the activator, the type of radiation detected, and the temperature. In general, the rise time is very fast: a few tenths of a nanosecond, and the fall time can be resolved into two components (Fig.A6.9):

- a prompt, exponential component with a time constant from a few hundred nanoseconds to a few microseconds
- a delayed component lasting several microseconds.

In NaI(Tl) the prompt component has a decay time constant of about 350 ns at very low concentrations of Tl, decreasing to 230 ns at normal concentrations (0.1% to 0.5%).

The fact that the delayed component may account for as much as 20% to 40% of the total emission of inorganic scintillators sets a limit to their usefulness in high-count-rate applications.

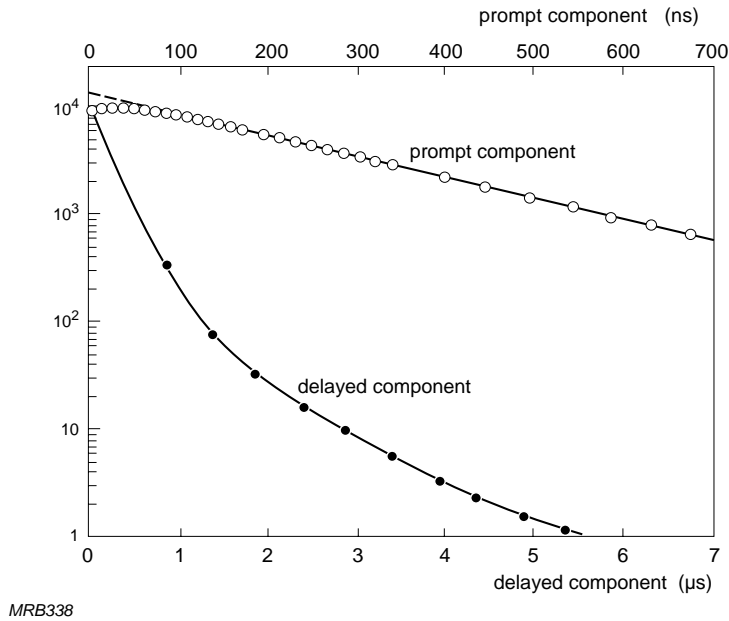


Fig.A6.9 Decay time components of a NaI(Tl) scintillator for γ -radiation
(*Rev. Sci. Instr.* 32 (1952) 1044)

Temperature effects. Temperature influences scintillation effectiveness, pulse decay time and emission spectrum. Figure A6.10 shows the scintillation effectiveness of CsI(Tl), CsI(Na) and NaI(Tl) as functions of temperature; note that the effectiveness of NaI(Tl) has a conveniently broad maximum around 20 °C. For use at very low temperatures special fast photomultipliers are now feasible despite the increasing resistance of the photocathode layer.

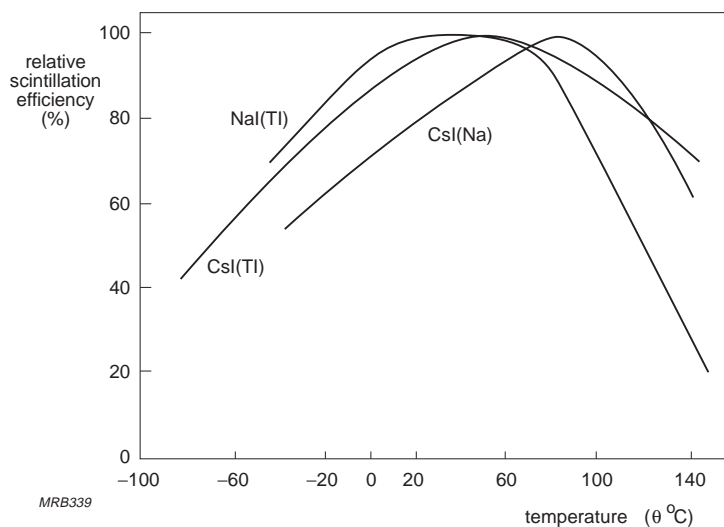


Fig.A6.10 Scintillation efficiency as a function of temperature for several inorganic scintillators (*Harshaw Chemical Company*)

Hygroscopy. NaI(Tl), CsI(Tl), CsI(Na), CsF, KI(Tl) and $^6\text{LiI}(\text{Eu})$ are all hygroscopic and have to be hermetically encased. BGO and BaF_2 , which are not hygroscopic, have high absorption coefficients for X- and γ -photons and very low delayed fluorescence. In some applications, such as medical PET scanners (Chapter 7), these properties compensate for the relatively low scintillation effectiveness of these materials. The new non-hygroscopic LSO scintillator, with a much shorter decay time constant than BGO and with similar stopping power, shows considerable improvements and therefore is the recent scintillator of choice for PET scanners. Other lutetium-based scintillators are under investigation worldwide.

A6.4.2 Organic-scintillator properties

Most organic scintillators are either monocrystalline compounds or liquid or plastic solutions.

Among the most efficient monocrystalline compounds are naphthalene, anthracene, fluoranthane, p-terphenyl (PT), p-quaterphenyl (PQ), and trans-stilbene.

Liquid scintillators are usually binary or ternary systems consisting of a solvent and small concentrations of one or two solutes that alter the emission wavelength. The most widely used solvents are alkyl benzenes such as xylene, benzene, toluene, etc. Common primary solutes are p-terphenyl, DPO, and PBD; common secondary solutes are POPOP, BBO, and BPO.

Chemically, plastic scintillators are very similar to liquid ones. Just as the alkyl benzenes are the most effective liquid solvents, their polymers, such as polyvinylbenzene, polyvinyltoluene, etc., are the most effective plastic ones. PT, DPO, and PBD are useful primary solutes for both liquid and plastic scintillators; common secondary solutes include BBO, TBP, POPOP, and DPS. An advantage of plastic scintillators is the ease with which they can be formed into a variety of shapes and sizes: the large scintillator sheets used in high-energy physics experiments are an example.

Table A6.3 compares the properties of some organic scintillators; in general, they have in common:

- high absorption for electrons and fast neutrons, but low γ -detection efficiency
- practically linear scintillation effectiveness over a wide energy range
- linear scintillation response for relativistic particles
- faster response than most inorganic scintillators.

Radiation absorption. Because of their comparatively low density (1 to 1.25 g/cm³) and the low atomic numbers of their constituent elements, organic scintillators are less absorbent for charged particles and X- and γ -photons than inorganic ones (Fig.A6.11). X- and γ -absorption, in particular, is nearly all due to Compton effect and can be increased by introducing a small concentration of a heavy-metal (e.g. Pb, Sn) organic salt.

Figure A6.12 shows the calculated path lengths of four types of particle in an organic scintillator. As the governing parameters, density and H/C ratio, are fairly similar in most organic scintillators, the path lengths do not differ much from one to another.

Because of their hydrogen content, organic scintillators are considerably more absorbent than inorganic ones for fast neutrons and are thus also used as neutron moderators.

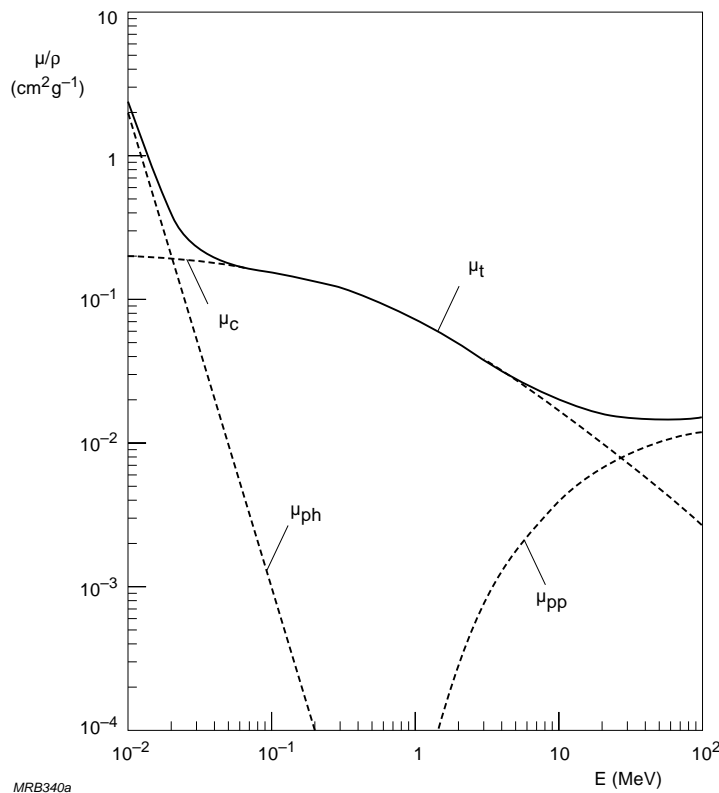


Fig.A6.11 Mass absorption coefficient for X- and γ -radiation in an organic anthracene C₁₄H₁₀ scintillator

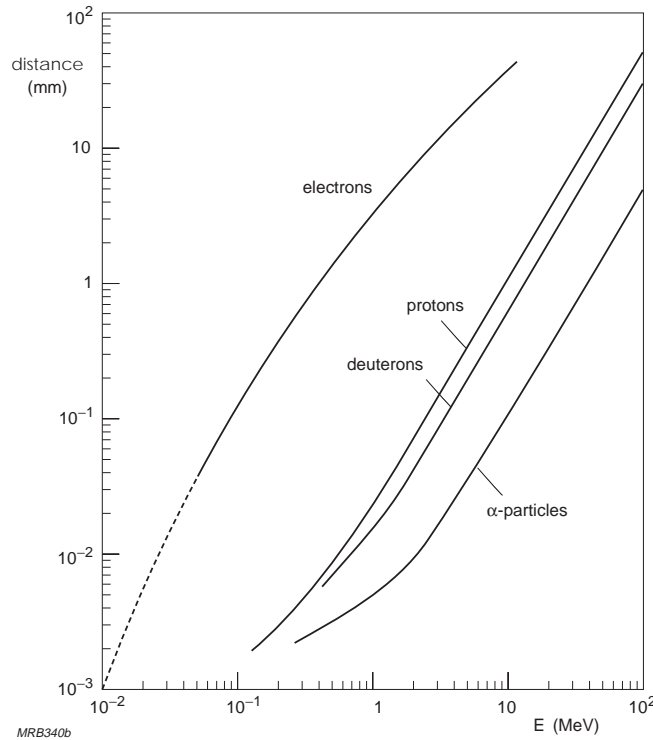


Fig.A6.12 Calculated pathlength of four types of charged particle in an organic scintillator (*Nuclear Enterprises Ltd.*)

Emission spectrum. The useful emission of most organic scintillators peaks at about 400 nm. Emission at shorter wavelengths is largely suppressed by auto-absorption due to overlap of the emission and absorption spectra (a wavelength shifting process with low Stoke's shift).

The emission of binary (single solute) liquid and plastic scintillators peaks at wavelengths below 400 nm. A small concentration of a secondary solute will shift the peak to between 400 nm and 500 nm where it is better matched to the spectral sensitivity of most photomultipliers.

The observable emission spectrum of plastic scintillators depends not only on the properties of the constituents but also on where the emission originates. Emission excited within about a micron of the output surface has a different spectral distribution from that originating in the interior of a (long) scintillator.

Transparency. Especially in large scintillators, transparency is of critical importance. Two factors that play an important part in it are selective absorption and multiple internal reflections; light intensity does not usually decrease exponentially with distance as Lambert's law would suggest. Therefore it is customary to characterize

the transparency of an organic scintillator by its half-thickness, the distance in which light intensity is halved. General information of organic scintillators can be found in manufacturers' catalogues.

Wavelength shifters (WLS) like BBQ, Y7, K27 etc. are plastics in which small concentrations of a secondary solute absorbs short-wavelength radiation, e.g. radiation peaking at around 400 nm, and re-emits it at a peak of around 500 to 550 nm. These materials are characterised by:

- a large Stoke's shift
- minimal overlap of absorption and emission spectra.

Here too (as with inorganic scintillators), an intensive search for new, superior materials is currently going on, driven by the needs of the physics community.

Sometimes, wavelength shifters are formed by evaporating organic materials onto the photomultiplier window. In this way, limeglass- or borosilicate-window tubes can be used to detect UV radiation (§6.1.3 and §8.3.1).

Table A6.3 Properties of some organic scintillators

scintillator	density (g/cm ³)	index of refraction	wavelength of maximum emission (nm)	decay time constant 1/e (ns)	scintillation pulse height ¹⁾	H/C ratio ²⁾
Monocrystals						
naphthalene	1.15	1.58	348	11	11	0.800
anthracene	1.25	1.59	448	30-32	100	0.714
trans-stilbene	1.16	1.58	384	3-8	46	0.857
p-terphenyl	1.23		391	6-12	30	0.778
Plastics ³⁾						
BC-400	1.032	1.581	423	2.4	65	1.103
BC-404	1.032	1.58	408	1.8	68	1.107
BC-408	1.032	1.58	425	2.1	64	1.104
BC-412	1.032	1.58	434	3.3	60	1.104
BC-414	1.032	1.58	392	1.8	68	1.110
BC-416	1.032	1.58	434	4.0	38	1.110
BC-418 (pilot-U)	1.032	1.58	391	1.4	67	1.100
BC-420	1.032	1.58	391	1.5	64	1.100
BC-422	1.032	1.58	370	1.6	55	1.102
BC-422Q	1.032	1.58	370	0.7	11	1.102
BC-428	1.032	1.58	480	12.5	36	1.103
BC-430	1.032	1.58	580	16.8	45	1.108
BC-434	1.049	1.58	425	2.2	60	0.995
BC444	1.032	1.58	428	285	41	1.109
BC470	1.037	1.58	423	2.4	46	1.098

¹⁾ relative to anthracene

²⁾ ratio of hydrogen to carbon atoms

³⁾ Saint Gobain Crystals & Detectors (Bicron), Newbury, Ohio, USA